Breast Modelling For Multi-Modal Mammographic Correspondence

David Raba Sánchez

Directors:

Dr. Robert Martí i Marly
Dra. Marta Peracaula i Bosch

Departament d'Electrònica, Informàtica i Automàtica

Institut d'Informàtica i Aplicacions

Universitat de Girona

"Biomechanics is mechanics applied to biology. The word 'mechanics' was used by Galileo as a subtitle to his book - Two New Sciences (1638) - to describe force, motion, and strength of materials... Biomechanics seeks to understand the mechanics of living systems. The motivation for research in this area comes from the realization that biology can no more be understood without biomechanics than an airplane can without aerodynamics. For an airplane, mechanics enables us to design its structure and predict its performance. For an organism, biomechanics helps us to understand its normal function, predict changes due to alterations, and propose methods of artificial intervention. Thus diagnosis, surgery, and prosthesis are closely associated with biomechanics."

Y.C. Fung [45]

Breast Modelling For
Multi-Modal Mammographic Correspondence

Contents

List of Figures

Chapter 1

Introduction

Among the different types of cancer, breast cancer has one of the largest incidences in the women population and is one of the most common causes of death in occidental countries. Given the hypothesis that a medical treatment is more effective in the early stages of cancer development, the use of tools aimed to provide an early diagnosis and an exact lesion localisation is of vital importance. In this Chapter, a brief review on breast cancer and imaging techniques will be presented.

1.1 Breast Cancer

Breast cancer is one of the most common cancer amongst women in western countries, while lung, liver, stomach, esophageal and bladder cancer affect primarily males. Worldwide, more than 700,000 women die of breast cancer annually and it is estimated that eight to twelve percent of women will develop breast cancer in their lifetime [56].

Medical diagnosis is commonly performed by external examination in the case of visible external abnormalities or by the analysis of images such as X-ray images. X-ray imaging is the most common modality used for the detection of breast cancer. Although in general it provides sufficient information, in some cases it is not conclusive and additional modalities which provide complementary information need to be used, such as magnetic resonance (MRI) and ultrasound (US) images. This practise is widely accepted by the medical community [26].

Meanwhile, other not so common modalities are also used by radiologists such as computed tomography (CT) and its recent improvements such as helicoidally CT, full field digital mammography (FFDM), Doppler based explorations, 3D ultrasound, electrical impedance tomography (EIT) among others. These image modalities coexist with a common aim to provide information which is not usually correlated with other tools used for the diagnosis. Nevertheless, absolute certainty about the malignancy of a tumour can only be obtained using invasive techniques. Among them, fine needle cytology aspiration (FNAC, MAMOTOMO and ABBI) is the least invasive and traumatic for the patient (compared to surgery). In such procedures there is a need to provide an accurate lesion localisation in order to precisely place the needle, an operation currently performed using US images or stereotactic systems. In the case of the abnormality is not visible in the US image, the correspondence between MR or X-ray images could provide a solution. This work aims to develop a tool which integrates (or fuses) the information from various modalities. Using such tools, a better and more accurate diagnosis and treatment could be provided.

The main goal of this work is to develop a complete framework for multi-modal image fusion based on the 3D realistic physical model of the breast obtained from the fusion of information provided by multi-modal images (such as X-ray mammography, Magnetic Resonance Imaging (MRI)). This model will take the complex features of breast compression, imaging procedures and internal changes into account.

1.1.1 Anatomy of the Breast

Knowledge of the normal anatomy on mammograms is very important in the diagnosis of breast disease. The size, shape, structure, and density of the breast are as variable as the female population. The breast is considered one organ with two mounds, often of symmetric structure. All components of the breast can change in normal and abnormal conditions, which is why interpretation of normality and abnormality is so difficult. Anatomically, the breast is composed exteriorly of skin and nipple and interiorly of galactophorous trees embedded in stroma containing connective tissue, fatty lobules, veins, arteries and lymphatic channels [47, 133]. Terminal ductal lobular units (TDLU) are found within these lobes, at the end of a tree structured duct system starting at the nipple. Figure 1.1 shows the internal

structure of a normal breast.

Breast cancer develops when abnormal breast cells begin to grow rapidly out of control. When a group of these cells band together, they form a mass called a *tumor*. Benign tumors do not spread and are usually not harmful. Malignant tumors, however, spread from their sources and can grow into life-threatening cancers.

When malignant cells leave the breast and invade other parts of the body (a process called *metastasis*) the chances of successfully treating the disease are greatly diminished.

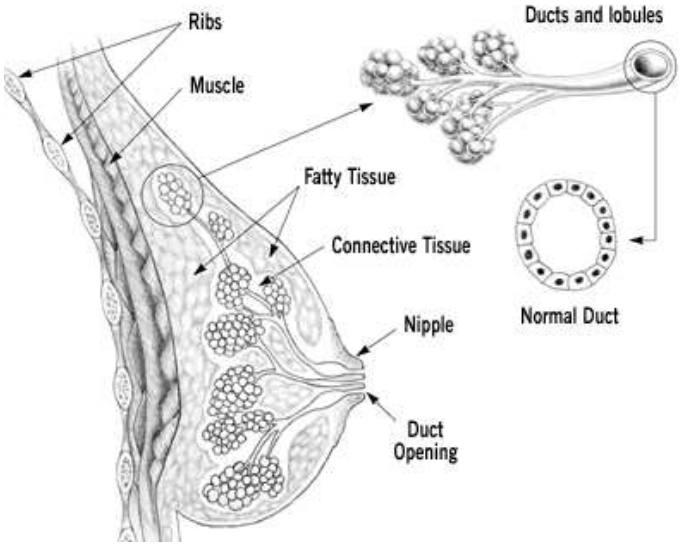

Figure 1.1: Breast anatomy with internal structure description.

The majority of breast cancers occur in women, but men can also develop the disease. Women are about 100 times more likely to be diagnosed with breast cancer, and factors relating to family history of breast cancer are known to affect breast cancer risk.

1.1.2 Breast Lesions

The breasts can develop various types of abnormalities. Some of them are related to certain anatomic structures, such as ductal carcinoma, that affects breast ducts whereas lobular carcinoma is localised in breast lobes. Breast carcinoma arise from stem cells which are thought to be located in the TLU and present the characteristics

of the tumour cell. Even so, not all changes or lumps in the breast tissue mean a breast cancer. In fact, the vast majority of breast conditions are not cancerous. Breast lesions may be associated with one of the following groups [133].

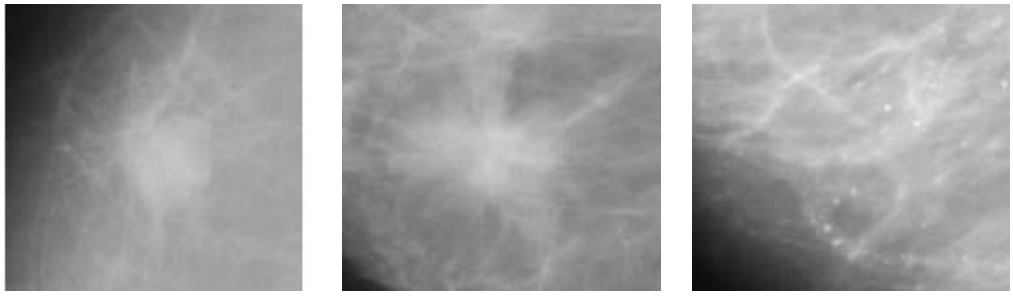

(a) (b) (c)

Figure 1.2: Types of X-ray mammographic lesions: (a) circumscribed and (b) spiculated lesions and (c) microcalcifications.

I. *Circumscribed lesions.* This type of lesion may present a sharp or poor outline and circular, oval or lobular shape. Diagnosis signs used by radiologists include contour, density, form, orientation and size. A halo sign, a sharp narrow radiolucent ring characteristic of benign growing tumours may be present in the contour. Also a capsule may occur, seen as a thin curved radiopaque line along the contour (this is generally a sign of a benign tumour). In addition, the contour density (grey-level intensity) of the lesion is also very important for its diagnosis. Basically, the density is compared to its surroundings to state whether it is radiolucent, low density or high density radiopaque or a combination of these [133]. Figure 1.2a shows an example of a circumscribed lesion.

II. *Stellate lesions.* A stellate lesion is characterised by a radiating pattern usually with an ill-defined contour. Diagnosis is carried out by analysing the presence, shape and density of a central tumour and the size and radiating pattern of the spicules. Radial scars are a type of benign stellate lesions with a very similar appearance which may lead to diagnosis errors. A spiculated lesion is shown in Figure 1.2b.

III. *Calcifications.* Most calcifications are benign (more than 80% of biopsied calcifications are not related to carcinoma). Diagnosis is achieved by deter-

mining their localisation (ductal or lobular) and performing analysis of their shape, size, density, number and distribution. Ductal calcifications in carcinoma are of irregular shape, small, dot shaped or elongated and irregularly grouped. Lobular calcifications are more homogeneous, dense with a sharp and generally spherical contour. Their distribution is more scattered than ductal calcifications. An example of calcifications is shown in Figure 1.2c.

IV. *Thickened skin syndrome.* Breast skin is inflamed increasing the breast size and weight due to a large fluid content. The overall breast density is also increased.

V. Any combination of two or more of the above.

1.2 Breast Imaging Modalities

Medical imaging has been an important part of medical diagnostics since the discovery of the X-ray in 1895. As the imaging technology has advanced in recent decades, applications of medical imaging have evolved to address increasingly complex disease states and conditions involving soft tissues and internal body organs. In order to understand the issues in medical image analysis, in contrast with processing of image of indoor environments or other structured environments we need an understanding of the salient characteristics of medical imagery.

This section provides a brief introduction to the most applied modalities in breast imaging. A high level description of the image formation in each modality is provided.

1.2.1 X-ray Mammography

Mainly used in screening programmes, screening mammography is based on a low-dose X-ray examination of the breast that is performed on women with no complaints or symptoms of breast cancer (asymptomatic). Generally three different views can be obtained with X-ray mammography: cranio-caudal (CC), medio-lateral (ML) and medio-lateral oblique (MLO), (Figure 1.3 shows two of the most common views). The goal of screening mammography is to detect breast cancer when it is still too

small to be felt by a physician or the patient. Research has shown that the early detection of small breast cancers by screening mammography greatly improves a woman's chances for successful treatment [64].

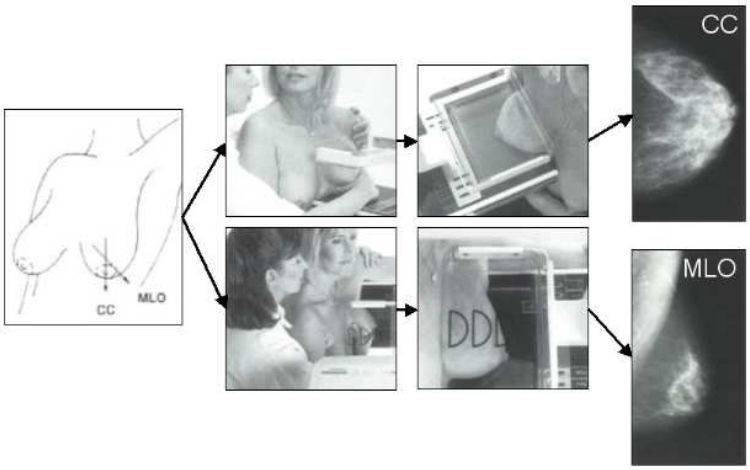

Figure 1.3: Common views in mammography: CC and MLO views from the same patient in both breasts. Typical image resolutions in digital systems are 2048x4096 and 12 bits per pixel.

This modality is obtained by short X-ray pulses which go through the imaging body and are captured by a special photographic film. The X-ray absorption is proportional to the density of the penetrated tissue (as seen in Figure 1.4). The X-ray absorption varies from bony structures (maximum) to fatty tissue (minimum). Images are obtained by compressing the breast and varying the X-ray incidence angle, usually obtaining two main views: cranio-caudal (CC, from top to bottom view) and medio-lateral oblique (MLO, lateral view).

The use of these two views is the common practise and often sufficient for the detection of the majority of the abnormalities. Due to the fact that it is an ionizing modality there is a need to minimise patient exposure. The generalised use of digital mammographic systems will greatly influence the image quality and will facilitate the integration with existing systems in medical centers such as PACS ("Picture Archive and Communication System"). Recent advances in mammographic imaging also incorporate computed tomography (CT and helicoidal CT) systems. This technology obtains images with an improved definition and has the advantage of not being projective. Nevertheless all those advantages are off-set by the increased

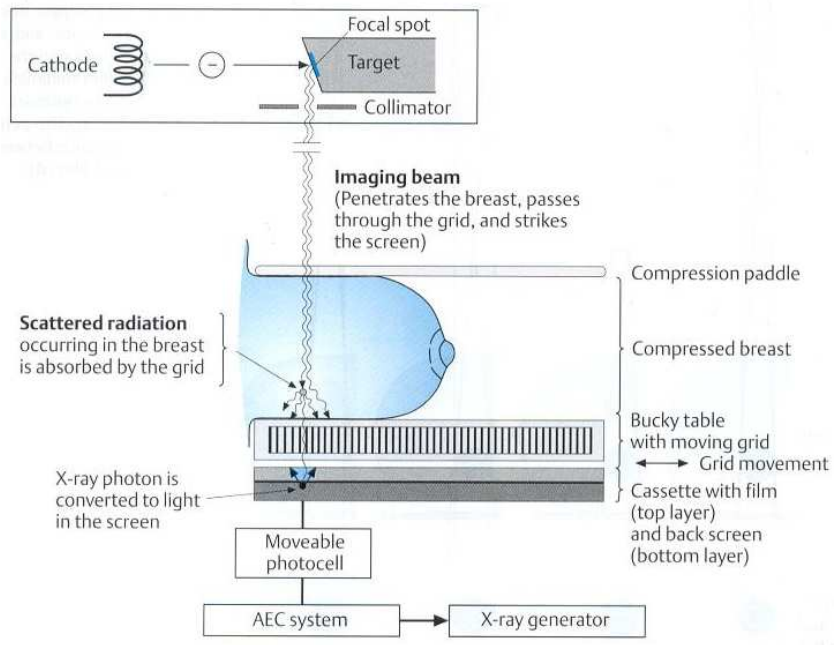

Figure 1.4: X-ray imaging process. Taken from [56].

ionising levels suffered by patients (about forty times greater than conventional mammography).

1.2.2 Magnetic Resonance Imaging

In 1946, Felix Bloch and Edward Purcell independently discovered that a magnetically energised substance bombarded with radio frequency (RF) emitted a "tune" similar to a diapason. They found that the nuclei of different atoms absorbed radio waves at different frequencies.

Magnetic resonance is based on capturing changes in the magnetic properties of protons in atomic nuclei induced by strong magnetic fields and radio frequency signals. Protons in a magnetic field (B_o) are aligned and counter aligned with it forming a net or macroscopic magnetisation. The application of a RF signal at a specific frequency (Larmor frequency) causes nuclei to jump into a higher energy state which induces a direction change in the net magnetisation away from the B_o field [107]. The magnitude of the generated signals are characteristic of each imaged tissue and their detection allows the formation of the MR image. Based on the

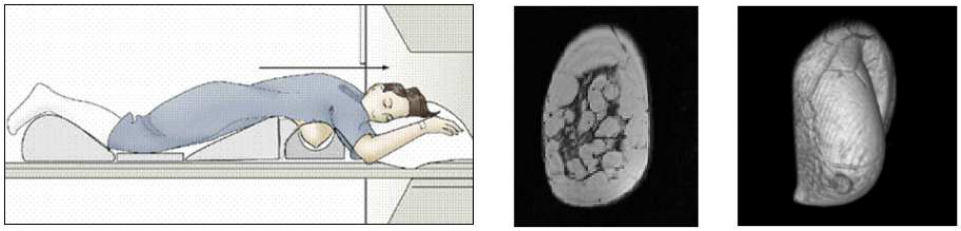

(a) (b) (c)

Figure 1.5: MRI: (a) breast MR imaging acquisition, (b) MR slice and (c) volume rendering. Typical slice resolutions around 256x256 or 512x512 and 8 bits per pixel.

study of hydrogen nuclei several slices are obtained (tomographic images) of the body. Images are obtained by placing the body inside an electro-magnet with a toroidal shape and emitting a given radiation. In the breast MRI acquisition, the patient lies facedown in the scanner with the breast pendulous and compressed or uncompressed in the breast coils (see Figure 1.5a) in contrast with mammographic, where the patient remains upright with one breast at time compressed between two plates. With this technique a volume of the breast can be obtained (a 3-D image in which the picture element is called *voxel*) showing a good contrast, no ionisation exposure and minimising the breast compression as shown in Figure 1.5b,c. However, MRI images show less resolution compared to X-ray (i.e. microcalcifications usually can not be seen). The main drawback is currently its high cost for being used in screening procedures.

MRI allows two types of studies: architectural and kinetic (also referred to as dynamic). Architectural studies on axial and/or sagittal planes are used to obtain morphological information about the lesion and its surroundings: location, shape, smoothness of contours and solid or liquid filled are often signs used by radiologists. Kinetic studies obtain an image of the breast before and after the injection of a contrast agent, generally Gadolinium DTPA, with a time interval that ranges from 6 to 12 minutes. The contrast agent increases contrast between malignant and benign lesions depending on their vascular properties. Lesions which acquire a high contrast rapidly (about 2 minutes after) and wash it out over the first 5 minutes are likely to represent cancer, whereas areas of constant increasing contrast are more likely to be reported as benign. It is widely accepted that kinetic and architectural features should be used in conjunction to achieve the highest accuracy on the diagnosis. Usually a subtraction between pre and post contrast images can be performed,

which will highlight lesions even more, assuming that the patient movement has been minimised during the procedure.

1.2.3 Ultrasound Imaging

First developed for military aims in World War II, the technique of sending sound waves through water and observing the returning echoes to characterise submerged objects, is now widely used in virtually every branch of medicine. Ultrasound imaging is based on the same principles as the sonar used by bats, ships at sea and fishers with fish detectors. When the ultrasound transducer is scanning the breast surface, it directs a stream of inaudible, high-frequency sound waves into the body. As the sound waves echo back from the body's fluids and tissues, the sensitive microphone in the transducer records the strength and character of the reflected waves [75].

It is commonly used as a first exploration method thanks to its easy acquisition and is specially indicated for the detection of masses but it is not regarded as a modality to be used for screening due to its low resolution and noisy images. Ultrasound provides some advantages compared with other imaging techniques as Magnetic Resonance or X-ray. Ultrasound is widely available, it uses no ionising radiation, Ultrasound can visualise structure, movement and function in the body's organs and blood vessels with no risks for standard diagnostic, there are no known harmful effects to humans. Ultrasound provides real-time imaging, making it a good tool for guiding minimally invasive procedures such as needle biopsies.

There are three major types of ultrasound imaging. The most commonly, the *B-mode (brightness) Ultrasound* beam is swept repeatedly over the area being examined, generating a series of 2-D images which show motion (see Figure 1.6a). Images are real-time, 2-D and gray-scale (solid areas in "white," fluid areas in "black"). In breast imaging, this modality provides tissue characterisation, lesion localisation, and also used to guide needle biopsies. As a second choice, *Doppler and Duplex Ultrasound* provide real-time coloured images, one-dimensional (spectral) or two-dimensional, most widely used in the analysis of blood flow to assess blood vessel or vascular functionality. Colour shades represent variations of blood flow, which is useful in breast cancer detection as nodes usually get more vascularised than other surrounding tissue (see Figure 1.6b). A third imaging technique is referred to *M-mode (motion) Ultrasound* which provides one-dimensional images, displaying

changes in the position of sound-reflecting structures over time. M-mode ultrasound applicability in breast diagnosis has not been yet assessed (see Figure 1.6c).

(a) (b) (c)

Figure 1.6: Ultrasound Imaging Modes: (a) B-mode, (b) Doppler imaging and (c) M-mode ultrasound.

1.2.4 Other Modalities

Other more uncommon techniques exist to assess the diagnosis of cancer. These are briefly reviewed as follows.

Dual-energy: Contrast Enhanced Mammography Contrast-enhanced digital subtraction mammography involves the injection of a non-ionic iodinated contrast agent to highlight new blood vessel development that accompanies malignant growth. First, two images are taken at different energy levels. The next step involves spatially registering the images to correct for non-rigid body movements of the breast between the first image and each image from the post-contrast image sequence [70]. The third step consists of a logarithmic subtraction of each warped image from the reference image (Figure 1.7 shows the main acquisition steps).

The analysis of the lesion is performed by a radiologist paying attention at morphology and the presence of enhancement, as well as to the analysis of the kinetics of the enhanced regions over the entire time sequence.

Full Field Breast Tomosynthesis One of new tools on the horizon for breast cancer detection is tomosynthesis. Current mammography generates a 2-D image of a 3-D structure by superimposing all structures in the path of incident X-ray beam on the detector [81]. Pathology of interest may be lost in the

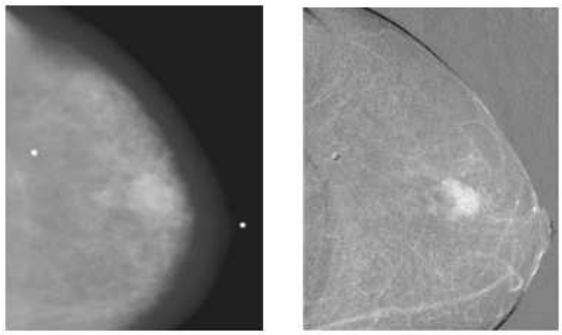

(a) (b)

Figure 1.7: Example of (a) pre-contrast image and (b) post-contrast image for a simple model of digital subtraction with dual energy mammography.

information superimposed by normal structures located both above and below. This is one factor which contributes to failure to diagnose certain breast cancers. The method of this 3-D image acquisition involves obtaining multiple snap shots of the stationary breast at multiple angles as can be seen in Figure 1.8.

Multiple breast tomosynthesis slices can be acquired at a dose equivalent to a single image conventional mammogram. Objects located at different heights in the breast will project differently in the different images obtained. The reconstruction of these multiple images generates information that enhances objects from a given height and blurs out objects at different heights. Images once reconstructed into thin high resolution slices may be viewed individually or in a cine (movie) mode.

There are many potential benefits anticipated from the addition of tomosynthesis as a breast diagnosis tool. It should be able to reduce the recall rate of patients as it reduces confusion which arises from tissue overlap. The biopsy rate should also be decreased as there is improvement in separation and visualisation of parenchymal structures. An additional benefit to some patients will include reduction in breast compression. During conventional imaging, compression is utilised to spread tissues and reduce overlap of structures thereby reducing confusing images. As the tomographic technique separates tissues primarily, a minimum amount of compression is required only to immobilise the breast. Time will possibly show improvement in cancer detection partic-

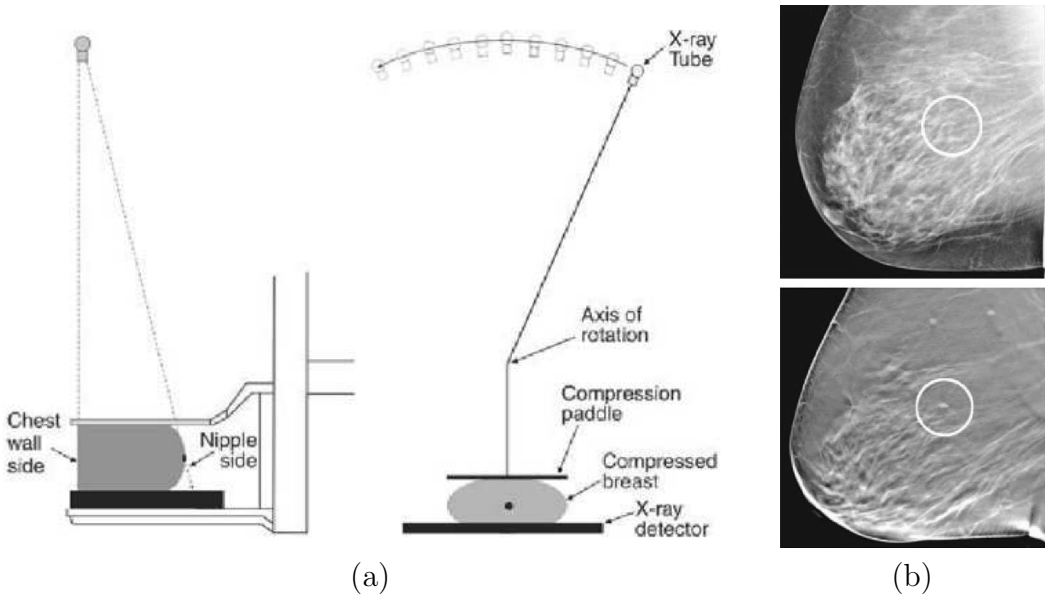

(a) (b)

Figure 1.8: (a) Schematic of the breast tomosynthesis acquisition system. Left: Side view. Right: Front view. (b) Example thomosynthesis images.

ularly in patients with dense breasts. Researchers are currently investigating the use of intravenous contrast to further improve the identification of breast cancer when used in conjunction with tomosynthesis.

New Upcoming Technologies Some other techniques are still under research or are not as widely used as the ones previously described. Although its application in breast imaging could be considered marginal, its results are promising and time will prove its effectiveness in breast cancer diagnosis.

- *Nuclear Imaging.* This includes both position emission tomography (PET) and single photon imaging (scintimammography). Scintimammography technique is usually applied when other modalities give no conclusive results. Imaging is performed using a gamma camera after the injection of a radiotracer (in the arm vein or foot, no injection is made in the breast). Both methods use radioactive tracers to identify regions in the body with altered increased metabolic activity. The preferential uptake of these tracers occurs because tumours metabolise at a higher rate than normal tissue. The images differentiate tissues based on the functional capacity of tissue behaviour. Normal breast tissue takes up very little

tracer, which allows metabolically active cancers to be easily spotted.

- *Elastography.* This imaging technique looks at only the elastic properties of tissues by applying a slight compression to the tissue and comparing an image obtained before and after compression. thic comparison is performed using a cross-correlation technique to determine the amount of displacement each small portion of tissue undergoes in response to the compression applied by the ultrasound transducer. The compression is very small, usually only 0.2 to 0.6 mm. The rate of displacement change the breast tissue as a function of distance from the transducer causing the compression is called a strain image and constitutes the elastogram. One area where elastography may be of great benefit is in distinguishing fibrosis of the breast from cancer. Preliminary work in elastography has shown that elastography can correctly classify most benign and malignant masses [32].
- *Bioelectric Imaging.* A low level of electric signal is introduced into the body using an electrode array on the surface. Sensors in a non-invasive probe are placed on the breast measuring the resulting electric field.
- *Near Infrared Optical Imaging and Breast Thermography.* An infrared camera is coupled with image processing hardware and software to track the temperature of blood as it flows into the breast and to identify areas of angiogenesis. An increase of temperature increasing is usually associated with an increase of vascularisation in malignant tumours.

1.3 Multimodality Imaging

The term multi-modality mammography refers to the use of a variety of mammographic modalities to provide a more accurate diagnostic for breast cancer. Different studies have shown that the use of various imaging modalities improves both sensitivity and specificity of the diagnostic [88]. Radiologists manually establish correspondence between areas in various modalities which is not an easy task and requires a high level of attention and training. The use of a methodology to perform it automatically could be very helpful in both reducing diagnosis time and errors and, moreover, could be used as a training tool for radiologists.

1.3.1 Related Work

Several research groups have been working on multi-modal image fusion. For instance, in the UK one should mention the Project "multi-modality medical fusion" from University College of London supervised by P. Ell, focusing on brain PET/CT and MRI/PET fusion [41]. Also, the same research group has been done interesting work on finite element models for evaluating image correspondence algorithms in mammograph [120]. A similar model was used by Ruiter [113] to find correspondence between MRI and X-ray images. Still in the UK, researchers at the University of East Anglia have published initial work on multi-modal mammographic image correspondence using MRI and X-ray images [90]. The medical imaging group of the medical school at the University of Rennes I (France) has also been researching on multi-modal images based on neurological applications and surgical simulations [68]. The Virtual Brain project at the University of Aalborg, proposes a brain model for training purposes obtained from multi-modal images (MR, CT and X-ray). Researchers at the University of Toronto (Canada) have published several works on physic models applied to mammography based on MRI information [116]. A similar work has been published coming from people at the Medical University Center in Pennsylvania (USA) using finite element models to construct a breast model in order to take realistic compression changes into account [5]. A complete and interesting review on multi-modality image fusion can be found in [105]. Is worth mentioning the work by Viola [141] on mutual information, Warner *et al.* [143] who proposed methods for using various modalities in mammography and the work by Piron *et al.* [103] from the University of Toronto (Canada) focusing on MR and US image fusion for breast biopsy. Similarly, Jenne *et al.* [69] from the University of Heidelberg (Germany) published work on MR and US imaging. In our country, although not entirely related to multi-modality mammography, there are various groups working on image analysis: the medical image lab at the Hospital General Universitario Gregorio Marañón, publishing interesting work on telemedicine, ultrasound and MR imaging, multi-modal image fusion in neurology [38, 117]. Another group is the Medical Image and Radiological Diagnosis Lab at the Universidad de la Coruña working on digital radiology, telemedicine and advanced medical visualisation. Finally, the research groups at the Universidad de Santiago de Compostela and the Universidad de Málaga where CAD systems for mammography, thoracic radiology, archiver systems (PACS) and quality control in radiology are their main

research topics.

1.4 The Use of CAD Systems for Breast Cancer Diagnosis

Mammography is one of the most effective methods for the early detection of breast cancer [39]. In recent years, is clearly noticeable the expansion of screening programmes in most of the occidental countries which has had an important impact on the survival rate for women with breast cancer [124, 145]. However, the number of women developing a breast cancer which is detectable using clinical or mammographic methods is only a small percentage of women that present an abnormality which is not clinically visible [57]. Therefore, novel strategies need to be developed in order to achieve an early detection, especially in women with a high risk of developing invasive breast cancer, with the corresponding therapeutic and social advantages this could introduce [79]. In this sense, is commonly accepted in the scientific and medical community that the use of CAD systems in the early diagnosis stages could provide an increased survival rate for those women affected with this neoplasia [96, 99]. Therefore, a tendency for fighting against cancer is the increasingly incorporation of novel techniques for the early detection of characteristic elements of cancerous symptomatology. Regardless of this tendency, one should admit that most medical centers working on the detection of mammary neoplasias in our country do not have computer aided tools and the current methodology is based on a visual inspection of the mammographic images by a group of experienced radiologists. A diagnosis in terms of grading the malignancy is given based on, among other information, the evaluation of a set of parameters relative to the mammary tissue. Thus, in addition to patient related information such as family history, child birth, age, hormone therapy or menstruation among others, a significant importance is given to specific elements of the image such as microcalcifications (number, shape features, texture, etc.), masses (density, shape and texture) or the presence of spiculated lesions. Nevertheless, in some occasions, some cancers are missed (or lesions incorrectly localised) by radiologists using visual inspection, even if symptoms are present in some of the multi-modal images. This lack of precision in the diagnosis could be due to different aspects, such as the subtle nature of the structures, a low

quality of the images or the visual fatigue of the radiologists among others.

The development of CAD (Computer Aided Diagnosis) systems used in medical applications is an important research topic in recent years in computer applied fields, such as computer vision and artificial intelligence. Most of those systems are designed to act as a second reader, with the poor confidence and misbelieve that such a system could rise in both medical professionals and patients. Hence, recent developments and experiments in CAD systems seem to focus on systems that do not aim to give a second diagnosis but provide radiologists with tools to facilitate and make their diagnosis more efficient. In conclusion, and taking those facts into account, the development computer aided diagnosis (CAD) systems is an important research area which is getting, and should get in the near future, a rising attention by the research and medical community.

1.5 Previous Work

The research presented in this report is related to the medical image analysis research developed by the computer vision and robotics group (VICOROB) at the University of Girona. Members of VICOROB have been working in a recognised way in medical imaging since year 1996, when they obtained their first funded project.

Currently, members of VICOROB, of medical research at the Hospital "Josep Trueta" and the Ramon Llull University are working in the third year of the project "HRIMAC" (Herramienta de Recuperación de Imágenes Mamográficas por Análisis de Contenido para el asesoramiento en el diagnóstico del cáncer de mama). HRIMAC is a content based image retrieval system based on mammographic images. Given a query image (patient case) which is being diagnosed, the system searches similar cases with a known diagnosis in a mammographic database. This similarity criterion is based on the contents of the image (presence of abnormalities, tissue type) but also on patient information such as age, number of children or breast cancer history. Thus, the system provides similar cases to the radiologist in order to provide a valuable help for achieving a better diagnosis (see Figure 1.9 for an overview of the behaviour).

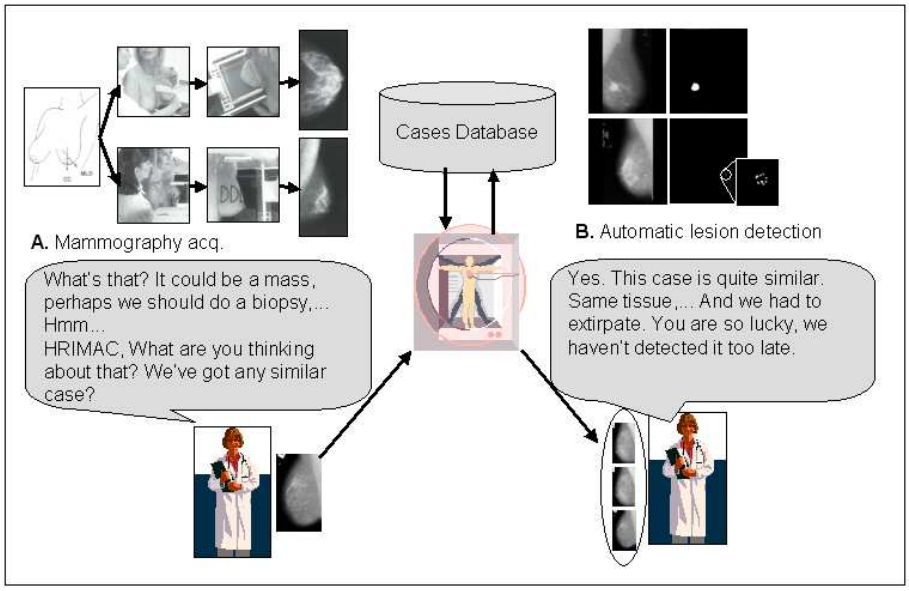

Figure 1.9: HRIMAC: Content Based Mammographic Image Retrieval.

1.6 An Overview of the Research Survey

As initially has been stated, the main goal of this work is to develop a complete framework for multi-modal image fusion based on the 3D realistic physical model of the breast obtained from the fusion of information provided by multi-modal images (such as X-ray or MRI). Following the structure of this research report, the work is presented in seven chapters.

The initial objective of corresponding MR imaging and X-ray mammography motivates the Chapter 2, which describes various approaches to obtain correspondence between this two breast image modalities. As a result of this Chapter, we conclude the need for a realistic simulation of internal breast tissue deformation. This deformation model should cover the complex features of breast compression, imaging procedures and internal changes. These are the motivation of Chapters 3 and 4. Chapter 3 reviews existing deformable models that could be used for breast tissue modelling, and Chapter 4 analyses different feature extraction approaches for mammographic images, making especial emphasis on breast profile and tissue classification which are needed for building the model.

As an initial step of building such a model, Chapter 5 presents on-going work

towards obtaining an accurate breast model. Chapter 6 describes the different objectives of the research thesis which are planned to be developed specifying the schedule and expected dissemination in conferences and journals. Finally, Chapter 7 presents published work of the author related to this research.

Chapter 2

Multi-modal Mammographic Registration

Image registration (also known as image correspondence) is the process of establishing point-to-point correspondence between two images. This chapter analyses the existing approaches that specifically tackle the correspondence problem between X-ray mammography to MR data of the breast.

2.1 Introduction

In computer vision, the image registration process is needed in various environments, such as stereo depth perception, motion analysis, change detection, object localisation and object recognition among others. Sometimes, relevant information comes from the same object that is imaged in a set of pictures. The problem appears when the capture conditions vary between images, due to changes in the viewpoint or object motion within the scene. Thus, given a similarity function that measures the matching rate between two images, image registration consists on finding the deformation that should be applied to maximise this similarity, or in other words, consists on aligning the object of interest in both images.

Breast imaging is an area where image registration plays an important role in the early detection of cancers. Radiologists often have difficulty locating and accurately identifying cancer tissue. X-ray mammographic image registration is usually done

on temporal studies, mammograms acquired from the same patient and the same breast, spaced in time for a period from six months to some years, in order to detect changes in the internal tissue structure. Change detection is not an easy task due to the X-ray acquisition nature, as the compression applied during the imaging technique produce changes in the tissue distribution which are directly projected on the X-ray image. Hence, the same structures in the initial image could displace its position only due to compression changes, as can be seen in Figure 2.1.

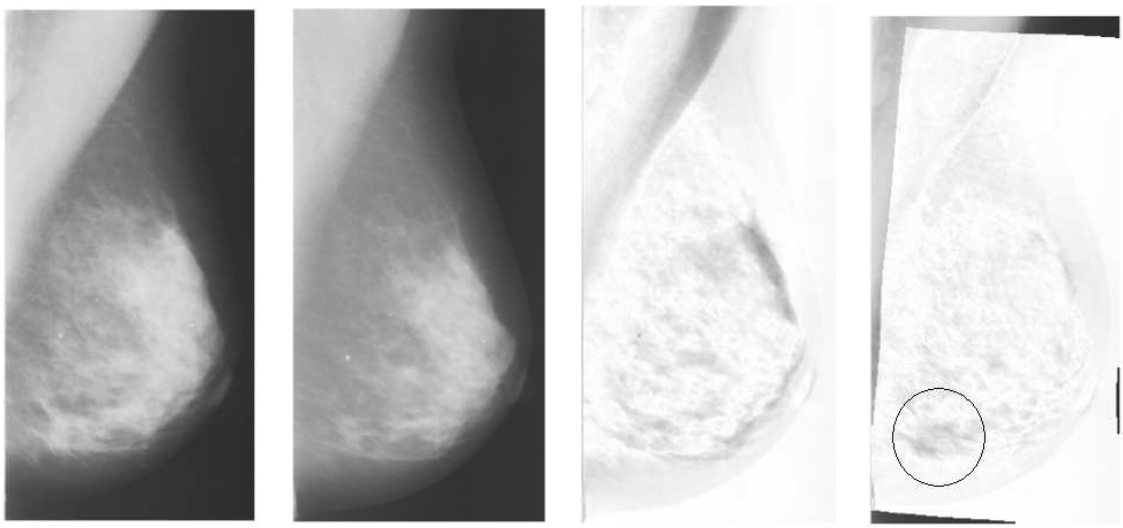

(a) (b) (c) (d)

Figure 2.1: Sample of temporal study with X-ray mammography, where (a) is the current mammogram and (b) previous mammogram. The direct intensity difference (c) of the pair of mammograms does not reveal the real changes, while the registered one (d) does, as denoted by the black circle.

Image registration is also applied on MR studies, where the information that should be registered increases its dimensionality to 3-D volumes. Registration has generally been applied to dynamic sequences corresponding a pre-contrast volume to a volume after a contrast agent has been injected. The injection of a contrast agent has the property of enhancing highly vascularised regions which is characteristic of malignant regions. In those studies, the patient movement is common because MR acquisition is a relatively long procedure (about 10 minutes). Hence, image registration is a key processing step to improve diagnosing results.

Several works on registration of images from different modalities have been published. Therefore, multi-modal registration is not a new challenge for non mam-

mographic medical applications such as brain multi-modal correspondence where successful approaches have been presented. A wide range of imaging techniques as computed tomography (CT), magnetic resonance imaging (MRI), positron emission tomography (PET) and single photon emission computer tomography (SPECT) have been combined. Multi-modal fusion in brain imaging usually takes advantage of the assumption of the brain as a rigid body, which obviously does not hold in mammographic images. Some of the assumptions done in other medical fields, as brain, lung or prostate disease, are not appropriated in breast multi-modal fusion, mainly due to the different compression rates between modalities.

Commonly used methods in multi-modal correlation are based on maximising a given similarity measure to obtain transformation parameters. Results obtained holds a high dependence on the chosen metric, that must be robust enough to provide a reliable measure of similarity. Excellent surveys on image registration are reviewed extensively in [87, 156], which cover specifically 2-D/2-D and 3-D/3-D data registration.

There are few works presented that deal with 2-D/3-D registration in breast imaging until now. The strategies can be described as follow:

- A first approach is to construct a 3-D model from X-ray images using different views and subsequently match this model with the MR volume [58, 114, 151].
- A second methodology involves the generation of projection from the 3-D MR data over a plane simulating the standard X-ray procedure and finding the areas which match the real X-ray image. The next step should be to correlate the MR projection with the real 3-D MR data [11, 90, 113].

Both approaches seem to be valid and involve common issues such as the model of the breast compression in different views (in both X-ray and MR modalities). Existing multi-modal mammographic techniques investigating correspondence between 2-D (X-ray) to 3-D (MR data) can be summarised in three main approaches: Behrenbruch *et al.* [11], Martí *et al.* [90] and Ruiter *et al.* [113, 114].

In the following section we will review three published approaches on X-ray/MRI correspondence. Although other similar and more recent works [108] have been proposed, these only reproduce the experiments proposed by the three selected approaches.

2.2 A_1: Pharmacokinetical Projection

Behrenbruch *et al.* [11] presented their approach in 2003. They tackle the problem of matching particular areas of an X-ray image using pharmacokinetic (2-D) projection of the MR volume and subsequently correlate the X-ray image with the full MRI volume.

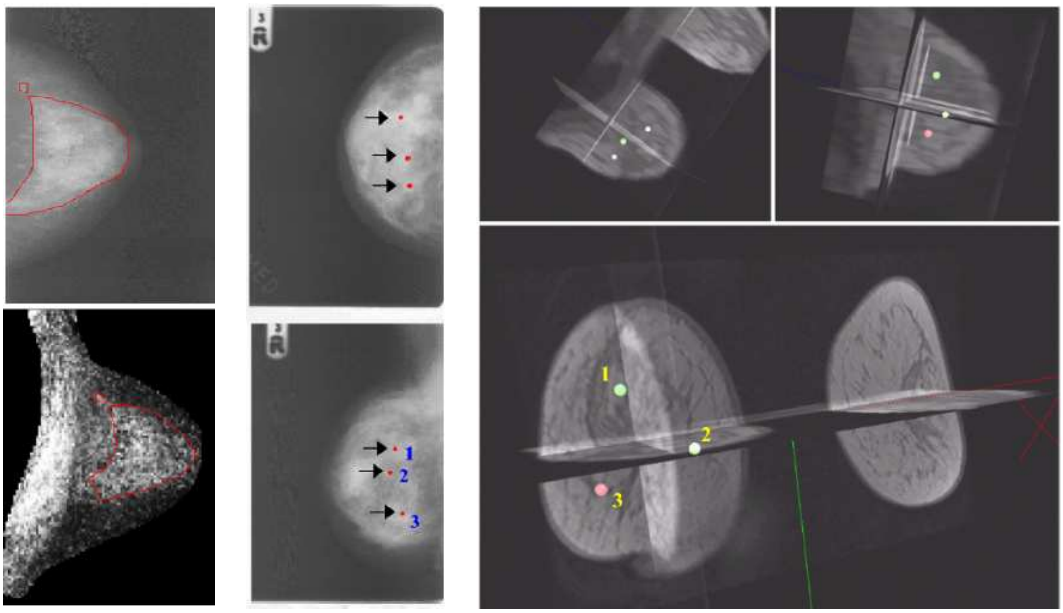

(a) (b) (c)

Figure 2.2: Behrenbruch's approach correspondence results: (a) pharmacokinetic (2-D) projection of the MR volume, (b) lesion localisation in X-ray images and (c) its correspondence in MR volume.

The key characteristic in this work comes from the projection model and the internal landmark detection. The projection step consists on creating an image from an MRI breast volume that is geometrically comparable to a X-ray mammogram. This projection represents the uncompressed breast shape. Instead of using a simple voxel direct summation method they use a projection based on pharmacokinetic principles, obtaining a projection similar to an enhanced mammogram. This is shown in Figure 2.2a. This pharmacokinetic model [20] describes the temporal behaviour of each tissue in contrast-enhanced MRI, that is the amount of contrast agent uptake during the acquisition of the MR images. The geometrical projection of the MRI using this model produces a *look-like-mammogram* image that tends to

enhance glandular tissue over fatty tissue.

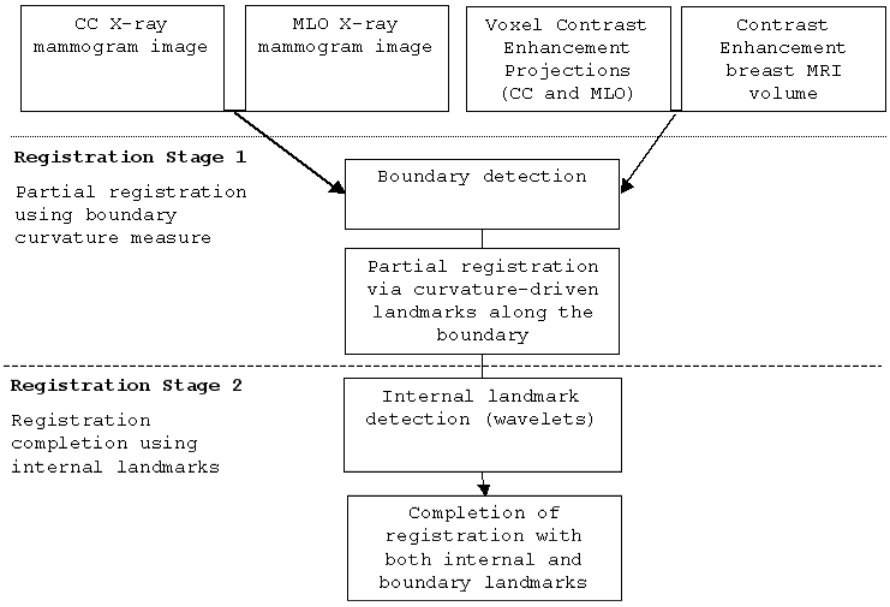

Figure 2.3: Behrenbruch's approach: Overview of X-Ray/MRI data fusion.

The X-ray mammogram is uncompressed registering it with the pharmacokinetic projection. The use of the uncompressed mammogram images allows an approximate volume reconstruction, and furthermore the comparison of pathologies that are visible in the mammogram with MRI. The localisation of a lesion in MRI volume starts with an intensity based approach with a spline interpolation to detect the breast profile in the X-ray image. A preliminary registration based on the boundaries deforms the X-ray mammogram until the shape of MRI projection is reached. In the second stage of the approach, the final registration is achieved adding a wavelet internal feature extraction process to the boundary features. Examples of correspondence are shown in Figure 2.2c where points represent areas of correspondence between MR and X-ray images. This approach does not take tissue deformation into account, hence it is not possible to predict internal tissue distribution under breast compression. This methodology is depicted in Figure 2.3.

2.3 A_2: Correspondence based on Linear Structures

The framework proposed by Martí *et al.* [90] in 2002 to register X-ray mammograms to MR volume is based on the extraction of internal linear structures from both X-ray and MR volume.

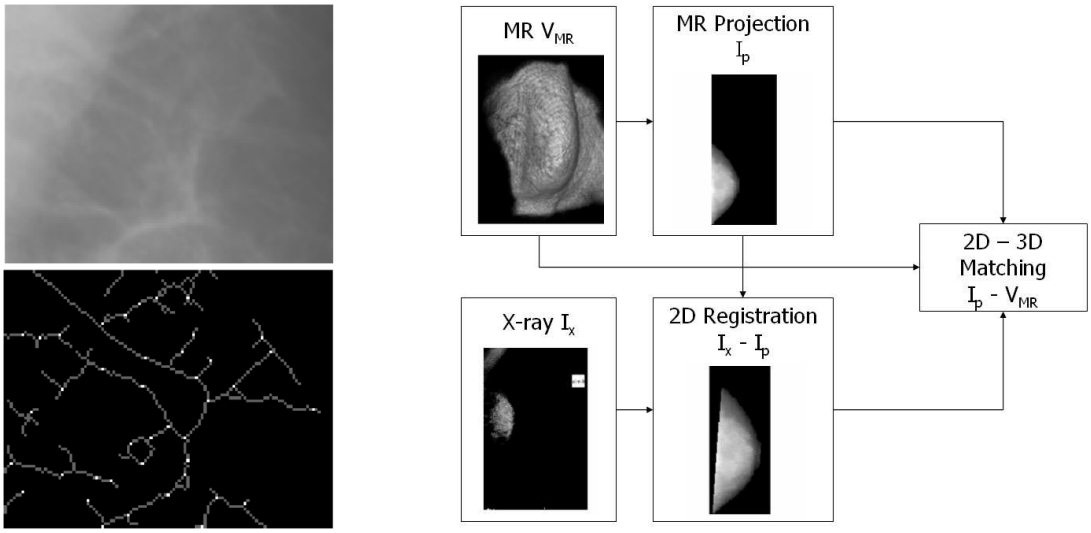

(a) (b)

Figure 2.4: Sample of (a) internal line structures detection and (b) X-ray to MR correspondence scheme.

An example of characteristic points extracted from mammographic images is shown in Figure 2.4a. Similarly to Behrenbruch approach, they project the MR volume to obtain a *look-like-mammogram* image. The difference with Behrenbruch approach is how the simulated mammogram is obtained. Initially the tissue types of the MR volume are classified using an EM approach into three classes, refined with a 3-D region growing approach based on intensity information. A *look-like-X-ray* image is generated using the tissue characteristics of the classified MR volume and a simple X-ray imaging model. In this model, the output intensity I of a beam of mono-energetic photons passing through a tissue of thickness x and density ρ is given by an exponential relationship shown in Equation 2.1.

$$I = I_0 exp\left(-\left(\frac{\mu_{fa}}{\rho_{fa}}\right)x_{fa} - \left(\frac{\mu_{gl}}{\rho_{gl}}\right)x_{gl}\right) \tag{2.1}$$

Where I_0 is the incident intensity, μ_{fa} and μ_{gl} are the attenuation coefficients of fatty and glandular tissues respectively, ρ_{fa} and ρ_{gl} are their densities and x_{fa} and x_{gl} their thickness. Values for μ_{fa}/ρ_{fa} and μ_{gl}/ρ_{gl} are obtained from *in-vivo* studies which tabulate the values for different kind of human tissues. The overall methodology is shown in Figures 2.5 and 2.4b.

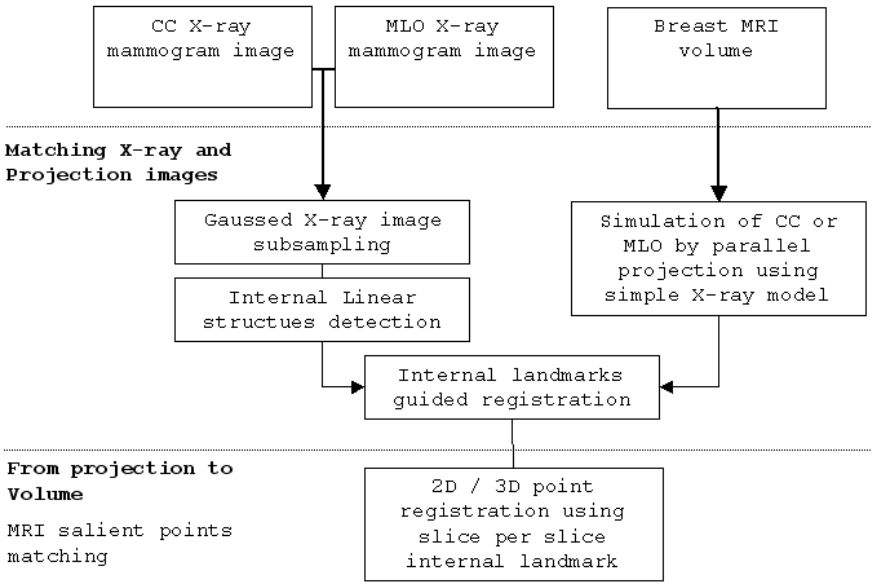

Figure 2.5: Martí's approach: Overview of X-Ray/MRI salient points correspondence.

A first registration step consists on correlating the MR projection with the original mammogram using a 2-D internal linear structures guided registration technique [91]. Corresponding points obtained in the 2-D registration are used to find their correspondence with 3-D salient points obtained with the same feature extraction process in the MR volume

Figure 2.6 shows an example of such matching: a point in the X-ray image is matched to a point in the MR volume using the described approach.

Evaluation is presented in terms of various experiments for a single case. Therefore the benefits of this approach can not be assessed until further evaluation is provided. In addition, no compression modelling is used, which could have a negative impact on the results.

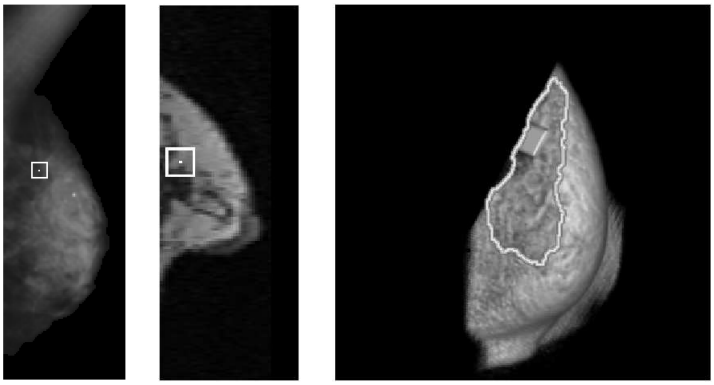

(a) (b) (c)

Figure 2.6: Example of X-ray to MR correspondence using internal structures: a point from (a) the X-ray image is matched to a point in the MR volume seen here as (b) a single slice and (c) a rendered volume. In all three cases the corresponding point is at the center of the square.

2.4 A_{3a}: Correspondence based on Maximising a Similarity Measure

Interesting works on breast multi-modal fusion can be found within Ruiter's publications [113, 114] since 2002. Her first proposal to cope with X-ray/MRI registration was in [114], where she proposed an elastic registration scheme.

To establish the three-dimensional position of a lesion, she starts with two mammographic views, which have to be uncompressed to look like an MRI-projection, the circumference of the X-ray is scaled as shown in Figure 2.7a, first in nipple direction and second in parallel chest direction. The inner structures are scaled using different scaling factors for each type of tissue (estimated from MR slice segmentation). With an initial estimation of the angle of the X-ray acquisition, and a given deviation, the best match between the uncompressed original X-ray mammogram and the MRI-projection is obtained by maximising a mutual information similarity measure with respect to the projection angle. As shown Figure 2.7b, spatial positioning can be easily located at the closer intersection point in the space of the projected lines from each lesion in the X-ray mammogram.

In this first approach, some basic assumptions are made: a) Relative distance of the tissue and the surrounding projection of the skin will remain constant during

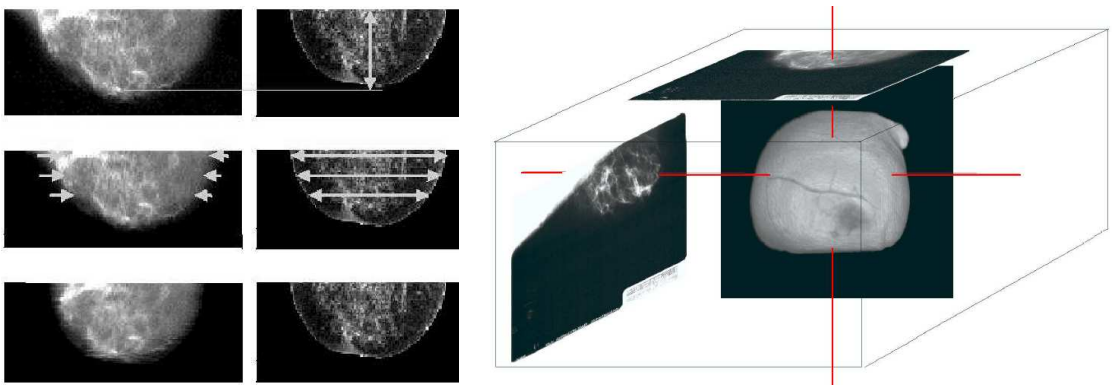

(a) (b)

Figure 2.7: Steps of the Ruiter's matching process. (a) Decompression of an MRI-projection. Top row, original CC X-ray image and 0º MRI-projection. Different length due to compression. Middle row: X-ray mammogram aligned to the length of the MRI projection. Different length due to compression, now, in parallel chest direction. Bottom row: final alignment. (b) Spatial correspondence between the MRI volume and two uncompressed X-ray mammograms. Lesion identified in both X-ray images, can be located at the closer intersection point in the space. Sample taken from [114].

every compression process, b) Projections of the undeformed breast (MRI) are seen as a special case of X-ray image, and c) Inner tissue displacements can be estimated from the behaviour of the shape of the projected breast as shown Figure 2.7a.

One could notice that this preliminary work lacks of correct tissue characterisation, which has negative repercussions in the accuracy. This subsequently included towards physical modelling of the breast compression, solving the low accuracy on tissue modelling, which is described in the next section.

2.5 A_{3b}: FEM Modelling Approach

The previously described approach was enhanced as a result of the research done in Ruiter's PhD thesis with the inclusion of a Finite Elements Modelling of the breast in 2004. This approach was to deal with the soft-tissue deformation [114, 113]. A 3-D simulation of the breast deformation based on a biomechanical model of the mammographic compression was used to register X-ray mammograms and MR volume.

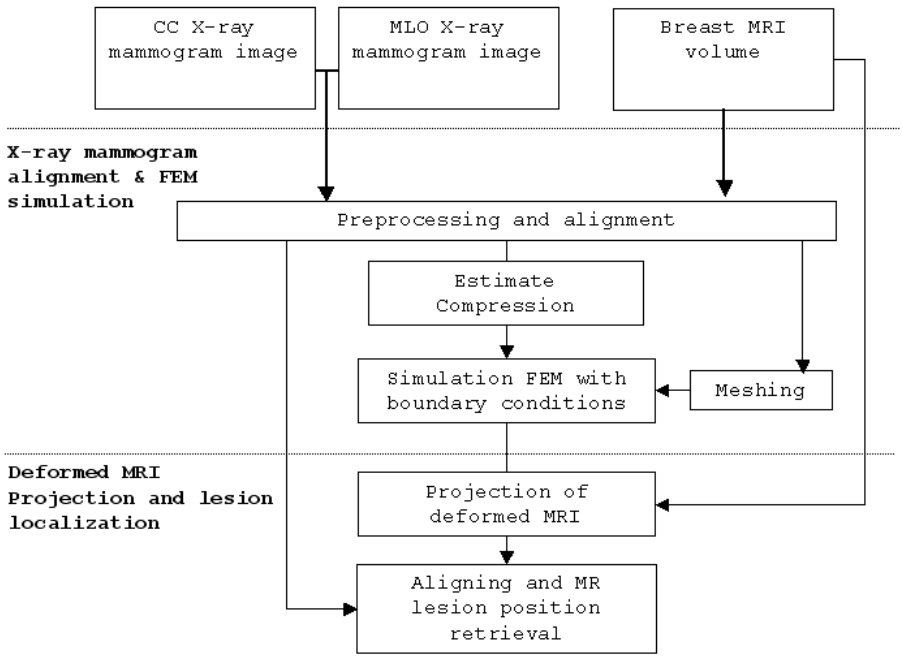

Figure 2.8: Ruiter's approach: Overview of X-ray/MRI correspondence using FEM deformation.

The registration starts with some preprocessing steps: The X-ray mammogram and the MR volume need to be segmented. Tissue characterisation is done using an EM [37] approach which segments each MR slice into three tissue types, breast profile segmentation is carried out manually and pectoral muscle in X-ray images is also manually removed, as it is not included in the simulation model. Next step consists on estimating the projection angle and the compression using the breast diameters. The simulation model is built based on the segmented MRI. This data is used for mesh generation, and provides the basis for building a Finite Elements Model. Tissue characterisation is based on a *neo-hookean* material model, which is the simplest nonlinear approach that models the elastic behaviour (see next Chapter for further explanation on deformation models).

The main aspects of the approach are shown in Figure 2.8. Hence, using the estimated compression and the projection angle they simulate the deformation via FEM, and obtain the MRI projection using this deformation. From here, the idea is the same as in her earlier work (Section 2.4). Now, a more accurate localisation of the lesion is achieved. Starting with the position of the lesion in a X-ray mammogram, they can estimate the projection line of the X-ray through the compressed

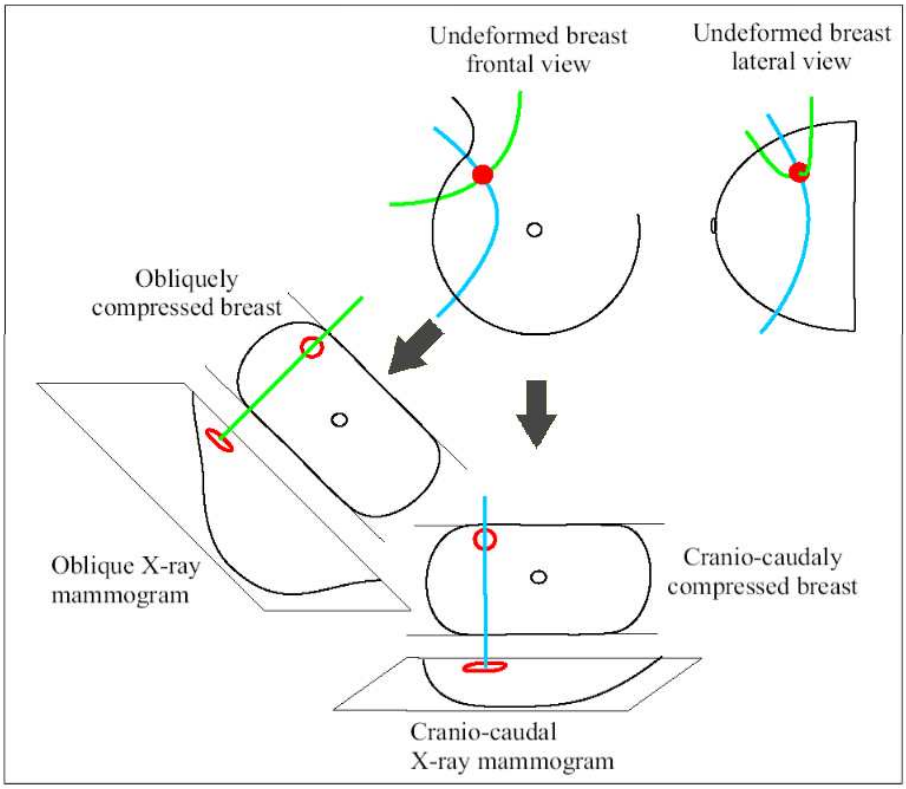

Figure 2.9: Ruiter's approach: Geometry of the lesion projection in different X-ray mammograms. Reprinted from [113].

breast. This line is uncompressed using an incremental search along the FEM, where candidates of the Finite Elements which might contain the point are chosen. Hence, a curve is created element by element from the compressed to the uncompressed form of the breast (see Figure 2.9). For a lesion visible in two X-ray mammograms, two curves can be drawn over the model and its intersection will be the lesion position. This does not exactly happen in real cases, thus, the closest intersecting point between the two curves is estimated.

Figure 2.10 shows examples of correspondence using her approach for real an synthetic cases. The main drawback of this methodology is the process of building the model itself as manual intervention is needed. In addition, such an accurate model like FE method build on unaccurated data as in this application needs to be justified in terms of computational cost by providing sound results. Recent work presented by Qiu [108] reproduces Ruiter's experiments in order to find lesion correspondence between CC and MLO X-ray mammogram views through the FEM.

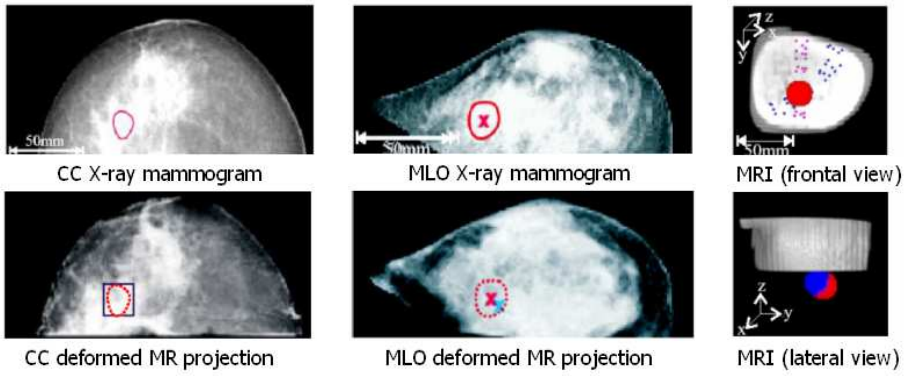

Figure 2.10: Ruiter's approach: Results of X-Ray/MRI correspondence using FEM deformation. Reprinted from [113] (a) CC and (b) MLO real correspondence and (c) a synthetic example.

2.6 Conclusions

This Chapter has reviewed the three most representative approaches for multi-modal mammographic registration. Their structure has been described and advantages and disadvantages of each method have been given. Table 2.1 summarises the main characteristics of each method describing their strong and weak points.

In summary, it is clear that a deformation model is necessary in order to describe the effects of compression. Other interesting issues are found in the presented approaches such the use of MR projections in order to match other modalities or the methodology used to correspond areas in X-ray and MR images (using boundary, internal structures or maximisation of a similarity function). Another important aspect, which to our opinion was not conveniently addressed in any of the reviewed approaches is the need of presenting significant evaluation results both in terms of accuracy and robustness using representative amounts of data. Comparison between methods is not a trivial issue, different image sources and prerequisites for its execution has been used in each method.

Next Chapter will be focused on deformable modelling techniques. Their study will be surely used to correctly model the breast anatomy.

A_1 **Pharmacokinetical Projection [11]**	
Description	Match pharmacokinetic (2-D) projection of the MR volume with particular areas of an X-ray image. Subsequently correlate the X-ray image with the full MRI volume using a wavelet internal feature extraction process to the boundary features.
Advantages	Incorporates lesion information from a pharmacokinetic model.
Disadvantages	Internal tissue displacements by compression are not modeled. Not realistically modelling the deformation. Only providing correspondence of detected lesions, not valid when a lesion is not present. Only tested qualitatively in a few cases.
A_2 **Linear Structures [90]**	
Description	Correlation of a MR projection with the original mammogram using a 2-D internal linear structures guided registration technique. Corresponding points obtained in the 2-D registration are used to find their correspondence with 3-D salient points obtained with the same feature extraction process in the MR volume.
Advantages	Using correspondence of internal tissue. Internal line structures present in both X-ray and MRI modalities. Quantitative matching evaluation is shown.
Disadvantages	Database is only one case. Not realistically modelling the deformation.
A_{3a} **Similarity Measure Maximization [114]**	
Description	Initially two X-ray views (CC and MLO) are registered with a simulated X-ray from MRI-projection. The best match between the uncompressed original X-ray mammogram and the MRI-projection is obtained by maximising a mutual information similarity measure with respect to the projection angle. Spatial positioning is located at the closer intersection point in the space of the projected lines from each lesion in the X-ray mammogram.
Advantages	Simple and intuitive approach.
Disadvantages	Internal tissue displacements by compression are not modeled. Linear approximation of deformations. Lesion localisation is needed in order to correspond the modalities. Few results.
A_{3b} **FEM Modelling [113]**	
Description	Finite Elements Modelling of the breast using MR volume. Lesion localisation estimating the projection line of the X-ray through the compressed breast. This line is uncompressed using an incremental search along the FEM, where candidates of the Finite Elements which might contain the point are chosen.
Advantages	Accurate simulation of the internal tissue displacement and lesion localisation. Quantitative results with synthetic and real cases.
Disadvantages	Manual intervention in model building. Feature extraction accuracy is not evaluated. High computational cost. Not realtime applicability. Not justified the use of FEM method.

Table 2.1: X-ray vs MR imaging correspondence models.

Chapter 3

Breast Biomechanics

After having reviewed X-ray and MR imaging correspondence techniques in the previous Chapter, it should be clear that a deformation model is essential in order to describe the effects of compression of breast tissue. In this Chapter, we briefly review the main techniques for modelling deformable objects, which have been and still are important research topics in computer graphics and medical imaging applications.

3.1 Introduction

Biomechanical modelling looks for the realistic simulation of soft tissue deformations under the load of external forces, assigning reliable physical properties to virtual anatomical structures in order to make them interact according to underlying physical laws. Modelling of biomechanical tissue properties has gained considerable interest in a range of clinical and research applications due to the new requirements on surgical planning, multi-modality management, image-guided procedures or simulation training. In addition, soft tissue modelling could also provide tactile sensation to human interaction trough cyber-surgical tool using haptic devices.

As described in Chapter 1, breasts are composed not only of glands but also of fat and fibrous tissue, which provides support and contains nerves as well as blood and lymphatic vessels. The mammographic compression due to imaging procedures deforms the breast structure, therefore it should be taken into account in order to understand and predict the distribution of the breast tissue and structural changes. Like other soft tissues, breast tissue shows a noteworthy capability to deform follow-

ing an elastic behaviour. Therefore, these characteristics force the simulation model to be capable of modelling a complex geometry composed of different non-linear materials and of simulating large deformations. There are few works that evaluate material properties of breast tissue, these publications describe as non-linear and uncompressible [5]. The elastic characteristics of tissue type are commonly derived from *in vitro* experiments [77, 144] with excised samples. In the above cited research one can also notice that *In vivo* material properties lamentably behave differently and can not be measured in the same manner [144]. Material properties estimations for tissue characterisation directly affect volume modelling. Different assumptions have been made for glandular and fatty tissue. For instance, Azar *et al.* [5] assume exponential behavior, Samani *et al.* [116] suppose hyperelastic and Bakic *et al.* [6] linear elastic stress-strain properties of the material models and all of them use different material parameters. The way internal tissue is modeled is a key issue to achieve an accurate simulation of the compression.

Breast modelling has been approached from different ways and different purposes. Firsts steps in breast modelling were done by works such as Yam *et al.* [151] where they obtained a 3-D reconstruction of microcalcification clusters from various mammographic views based on a compression model. This compression model was based on estimations about the deformation that the breast suffers using X-ray MLO and CC views [58]. Other models account for breast growing as in [136] and the use of a simplistic 3D breast tissue model as in [6] where synthetic mammograms are generated. Physical tissue characteristics have been introduced by various authors [5, 116, 119] with a common aim to realistically describe breast deformation under different conditions.

The remainder of this Chapter presents a review on various deformable modelling approaches (Section 3.2) with a special emphasis on physical models and finally some conclusions are given.

3.2 Deformable Volume Modelling

Deformable object modelling has been studied in computer graphics for more than three decades, across a wide range of applications. In Computer Aided Design and computer drawing applications, deformable models are used to create and edit com-

plex curves, surfaces, and solids. What we mean by modelling is the way objects or models can be represented, whether they are represented geometrically by mathematical procedures or abstractly by basic shapes and primitives. Modelling includes both the body material to be simulated and the way in which it will be manipulated. In image analysis, deformable models have been used to segment images and to fit curved surfaces to noisy image data, describe shape features, classifications, etc [27, 137]. Deformable models have been used in animation and computer graphics, particularly for the animation of clothing, facial expression, and human or animal characters. Surgical simulation and training systems demand both real-time and physically realistic modelling of complex, non-linear, deformable tissues. Interesting reviews on that subject can be found in [31, 35, 131].

Substantial work is needed to simulate realistic deformations in computer graphics, physics and medical environments. Reviewing the literature, two main methods are generally used to perform model deformations. One is based on mass-spring models [4, 25, 106] and the other is based on Finite Elements Modelling (FEM) simulations [5, 19, 138]. The mass-spring method is simple and fast, but offers less visual realism and accuracy whereas finite element methods can provide more realistic and accurate results, but are much slower to compute. More recent developments point to schema that provide real-time performance using adaptive modelling methods [34].

We describe some of the most commonly used techniques in deformation modelling classified in physical and non-physical modelling techniques (see Table 3.1 for an overview). While Non-physical approaches (Splines, Free Form Deformations, etc.) tends to give preference to user interaction and fast computation, Physical approaches (FEM, Mass-Springs, ChainMail, etc.) are founded on physical laws and provide more accurate and realistic modelling.

3.2.1 Non-physical Modelling

Providing accurate and realistic behaviour of our deformable model under external perturbations involves a solid physical and mathematical foundation. Nevertheless, many applications, particular in graphics and design environments, require computationally efficient techniques such as geometric modelling rather than heavy processing schemes. Several approaches exist which deal with deformable modelling

based on geometric deformation but usually undervaluing physical laws.

3.2.1.1 M_1: Geometric Deformable Models

Splines techniques are probably one of the earliest approaches for modelling deformable objects. Splines were essentially a designing tool based on interpolation curves and surfaces. To ease its manipulation other spline-based methods appeared in order to describe curves and surfaces by a small vector of numbers, including Bezier curves, B-splines, non-uniform rational B-splines (NURBS) and other types of spline definitions. The spline technique is based on the representation of planar and 3D curves and surfaces by a set of control points, also called landmarks. The main idea of spline based methods is to modify the shape of complex objects by varying the position of few control points. Also the number of landmarks as well as their weights can be used for adjustment of the object deformation [9]. Splines have been commonly used in elastic image registration frameworks based on functions which are derived from elasticity theory or from linear elastic solution of the thin-plate deformation problem [15].

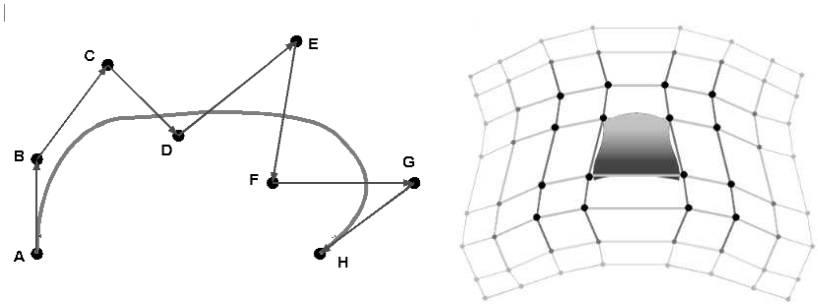

(a) (b)

Figure 3.1: Sample of (a) Spline and (b) Bezier patch.

Figure 3.1 shows an example of a spline (defined by its control points) and a Bezier Spline Patch defined by four points.

Free Form Deformation (FFD) was introduced in Computer Aided Geometric Design environments and animation as a geometric approach mainly based on Bezier-patches or splines [8]. A grid over the object modeled is defined and the deformations are produced according to transformation matrices applied to the grid. The main advantage is the low computation requirements. However, this is compensated with

low accuracy rates and the quasi-artistic development of a model due to the difficulty to express some deformations in terms of splines expressions or free-form mappings.

The formulation of a spline-based FFD over a volume $\Omega = \{(x, y, z)\}$ is as follows: Let ϕ denote a $n_x \times n_y \times n_z$ mesh of control points $\phi_{i+l,j+m,k+n}$ uniformly spaced. Thus, FFD can be written as the 3-D tensor product of the 1-D cubic B-splines.

$$FFD(x, y, z) = \sum_{l=0}^{3} \sum_{m=0}^{3} \sum_{n=0}^{3} B_l(u) B_m(v) B_n(w) \phi_{i+l,j+m,k+n} \tag{3.1}$$

where $i = \lfloor x/n_x \rfloor - 1$, $j = \lfloor y/n_y \rfloor - 1$, $k = \lfloor z/n_z \rfloor - 1$, $u = x/n_x - \lfloor x/n_x \rfloor$, $v = y/n_y - \lfloor y/n_y \rfloor$, $w = z/n_z - \lfloor z/n_z \rfloor$, and where B_l represents the lth control function of the B-spline [119] and defined as,

$$\begin{aligned} B_0(u) &= (1-u)^3/6 \\ B_1(u) &= (3u^3 - 6u + 4)/6 \\ B_2(u) &= (-3u^3 + 3u^2 + 3u + 1)/6 \\ B_3(u) &= u^3/6 \end{aligned} \tag{3.2}$$

B-Splines are locally controlled by a subset of points in ϕ, which makes them fast to compute for large number of control points. FFD have been used for non-rigid registration in image-guided surgery [112].

Geometric Deformable Models tend to penalise accuracy to speed up its visual response, reaching realtime capabilities. As a drawback, the accuracy of those methods is not comparable to physical modelling. In the following sections the most common physical methods are presented. From numerical engineering techniques such as Finite Elements Modelling to graphics environments such as Spring-Mass models, are used to accurately model a deformable object.

3.2.2 Physical Modelling

The application of external loads on an elastic body produces its deformation, and the removal of the external load means the restoration to its original shape. Realistic simulations of such behaviours on deformable objects involve physical modelling, hence an incursion in computational mechanics is unavoidable.

Models exist that are based on physical principles, also called *Non-continuum models*. They find an approximation to these physics, simplifying the representation and allowing fast computation. On the other hand, we can find physically based methods that deal directly with the equations of continuum mechanics. They are very accurate models but present expensive computation time and high memory requirements, they are known as *Continuum models*.

Theory of elasticity is the part of continuum mechanics that deals with elastic materials. Robert Hooke, announced the birth of elasticity theory. In 1675 he stated that the force applied on any body is proportional to its extension. Mathematically it is expressed as $F = k \cdot u$ where F is the applied force, u is the deformation of the elastic body subjected to the force F, and k is the spring constant. The linear Hooke law defines the easiest technique to model material behaviour. Unfortunately, material properties modeled such as uniformity, elasticity, plasticity, viscous materials contribute with complex equations and non-linear behaviours to the simulation. The nearer a physical model approaches the properties of a soft tissue the more realistic the simulation results can be obtained. The real tissue behaves as a linear Stress/Strain relationship model in case of small deformations. Beyond deformations larger than 10% of the volume more complex non-linear models are needed.

Stress, strain, equilibrium and displacement are the main concepts on elasticity, studying the relationship between forces and the deformations that they produce. *Stress* is the intensity of the force from interactions such as stretching, squeezing or twisting (force per unit area). *Strain* describes relative deformation or change in shape and size of the model under applied forces. When forces are applied to the tissue, it deforms to a configuration of points in which the energy of the tissue is in equilibrium. The unknown parameter is the displacement produced from the initial application of a force to the moment when the equilibrium is reached. There are two kinds of displacements, a) the rigid component, which means the displacement experienced if a constant distance between points is assumed and b) the strain. All the relationships between the body geometry, his material properties and the external loads, can be expressed in terms of energy variation, and therefore in terms of partial differential equations. The main drawback of these approaches is usually the computational cost, which should be approached using model simplifications or efficient numerical techniques.

In the remaining of this section we highlight the main approaches: Finite Ele-

ments Modelling, Boundary Elements Method, Particle Systems, Mass-Spring Models, 3D Chainmail and other Adaptive Models.

3.2.2.1 M_2: Finite Elements Modelling

The theory of Finite Elements Modelling (FEM) was first developed by M.J. Turner at Boeing over the period 1950-1962 and the main popularisers were J.H. Argyris, R.W. Clough, H.C. Martin, and O.C. Zienkiewicz whom are responsible for the "technology transfer" from the aerospace industry to a wider range of engineering applications during the 1950s and 1960s. A wide literature exists on Finite Elements Modelling method for engineering elasticity, however this literature has assumed mainly materials that undergo very small deformation within their elastic limits, such as metals, and is more concerned with distribution of forces, rather than the deformation itself. Biomedical applications are typically more interested on observable deformations of less rigid materials, such as soft tissue, organs, muscles or articulation movements. Even so this method is one of the most common approaches to model tissue deformable behaviour because its very accurate physical approximation.

The idea of using physics for computer animation was introduced by Terzopoulos [137] who proposed the use of elasticity theory for modelling deformable materials into the computer graphics applications. He used the FEM method to model elastically deformable objects and introduced some other interesting contributions as a coauthor. In medical environments, Chen *et al.* [24] developed a biomechanical FEM considering skeleton kinematics and physiological effect for muscle deformation and the pioneer work of Bro-Nielsen [19] who used FEM method in surgical simulations. For other applications like prostate imaging, FEM has been applied to predict deformation during needle insertion [76].

In FEM, the object deforms in a physically-based manner after solving the mathematical problem in response to external stimuli [19]. Finite Elements is a general theory to solve differential equations over some continuum. The basic concept is the subdivision of the volume occupied by a tissue before deformation, Ω, into non-overlapping components of simple geometry called finite elements. The response of each element is expressed in terms of a finite number of degrees of freedom characterised by the value of an unknown function, at a set of nodal points. A discrete

system of differential equations is generated for every element from a set of differential equations controlling the motion of material points of a continuum. The resulting equation then has to be integrated in relation to time. Using FEM, the equations that model the deformation are based on elasticity theory. Hence, next section briefly describes some concepts that should be taken into account in order to study soft tissue deformations.

Using elasticity theory, we model the object setting Ω as the set i nodes with position $x_i = [x, y, z]^T$ where $x_i \in \Omega$ and the displacement is defined in each node as $x_i + u_i(t)$.

This deformation is related to the application of external forces and object characteristics. Equation 3.3 shows the potential energy of the systems. Where E_{strain} is the strain energy and W_{ork} the work done by external loads. The potential energy (Π) is given by,

$$\Pi = E_{strain} - W_{ork} \tag{3.3}$$

Hence, the main idea in the FEM method is to calculate the total potential energy of the system, given by Equation 3.3, and minimize it by setting its derivative to zero and solving for the unknowns, the displacements of the nodes in equilibrium state. We define the W_{ork} as Equation 3.4, where f represents an external force.

$$W_{ork} = \int_{\Omega} f^T u dx \tag{3.4}$$

And E_{strain} is the energy of the linear elastic body Ω is shown in Equation 3.5 where ε is the stress vector indicating stress displacements relationships and σ is the strain vector.

$$E_{strain} = \frac{1}{2} \int_{\Omega} \varepsilon^T \sigma dx \tag{3.5}$$

We also define the stress vector ε as $\varepsilon = Bu$ where B is:

$$B = \begin{bmatrix} \frac{\delta}{\delta x} & 0 & 0 \\ 0 & \frac{\delta}{\delta y} & 0 \\ 0 & 0 & \frac{\delta}{\delta z} \\ \frac{\delta}{\delta y} & \frac{\delta}{\delta x} & 0 \\ \frac{\delta y}{\delta z} & 0 & \frac{\delta}{\delta x} \\ 0 & \frac{\delta}{\delta z} & \frac{\delta}{\delta y} \end{bmatrix} \tag{3.6}$$

The strain vector σ is defined as $\sigma = C\varepsilon$ using Hooke's law (a linear approximation). Material characteristics are modeled in the matrix C (Equation 3.7), which assume an homogeneous material.

$$C = \begin{bmatrix} \lambda + 2\mu & \lambda & \lambda & 0 & 0 & 0 \\ \lambda & \lambda + 2\mu & \lambda & 0 & 0 & 0 \\ \lambda & \lambda & \lambda + 2\mu & 0 & 0 & 0 \\ 0 & 0 & 0 & \lambda & 0 & 0 \\ 0 & 0 & 0 & 0 & \lambda & 0 \\ 0 & 0 & 0 & 0 & 0 & \lambda \end{bmatrix} \tag{3.7}$$

Material parameters are expressed in terms of Young's modulus E and the Poissons ratio σ. They are related to λ and μ parameters of matrix C (known as the Lamé parameters) by the following equations.

$$\lambda = \frac{\sigma E}{(1+\sigma)(1-2\sigma)} \tag{3.8}$$

$$\mu = \frac{E}{2(1+\sigma)} \tag{3.9}$$

Young's modulus represents the stiffness and Poisons ratio the compressibility. The closer σ it to 0.5 the more incompressible the material is. Then the energy function is:

$$E(u) = \frac{1}{2}\int_{\Omega} (uB)^T CBudx - \int_{\Omega} f^T udx \tag{3.10}$$

To calculate this integral, the Ω continuum is discretised into elements joined at node points as shown in Figure 3.2. The element type chosen and the interpolation

function of the displacement field defined determine the FE configuration. The most commonly used element type is a tetrahedral element with a linear interpolation on the four nodes.

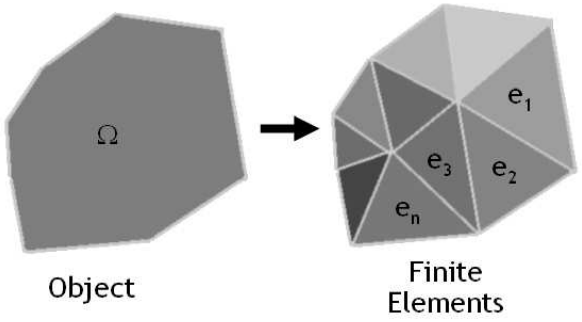

Figure 3.2: Uniform discretization of the shape Ω into triangle elements.

Summarizing, the system consists of the deformable tissue and the loads that act on it. Thus, the total potential energy of the system is the stain energy of the deformed object minus the potential energy lost by the loads corresponding to the work of deforming the volume. We define E_{strain} as the strain energy of the object, W_{ork} is the work done by the loads, and Π is the total potential energy of the system. Thus, we need to express E_{strain} and W_{ork} in terms of the displacements, the unknowns. The equilibrium equation is written for each element, and finally these equations are aggregated into one large system of equations. FEM treats a problem in a continuous manner, but solved for each element in a discrete way, this is computationally expensive but the main advantage of FEM is that they can produce more physically realistic simulations compared with other approaches. A key characteristic is the application of boundary conditions which has several purposes: (a) To ensure simulation of local or global continuum symmetry, (b) to avoid unintended deformations, (c) to constraint the position of the body in the space, and (d) to apply the sitting pressure of the body uniformly distributed.

Explicit FEM

In order to reach the mentioned greater physical accuracy, FEM has been applied to models derived from elasticity theory, but requires solving a large sparse equation system. FEM method requires high computation, and undesirably, the reduction in the number of nodes will reduce its computational cost, but in turn degrade the accuracy of the model. The use of mathematical tricks such as matrix invertion

and pre-computations obtains computation times that draw near to real-time requirements of simplified models [19]. These modifications have undesirable but less pronounced repercussions in the accuracy of the model.

Another approach using elasticity theory and derived from FEM is sometimes referred as *Explicit Finite Elements* [36], which consist on a spatial discretisation. FEM techniques split the object into elements on which the physical equations are expressed. Instead of merging all these equations in a huge matrix system, explicit FEM solve each element independently through a local approximation. It is a method less accurate than FEM but obtains a significant reduction on computation time (see Figure 3.3 for an illustration).

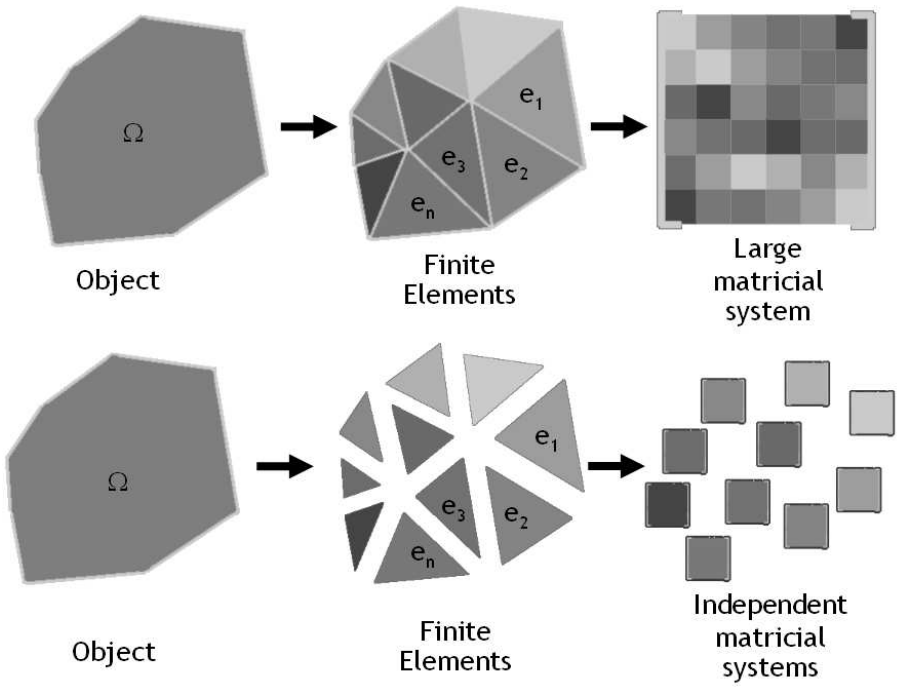

Figure 3.3: The classical FEM discretisation and matricial system formation (first row) *versus* the Explicit FEM formulation (second row). Based on [65].

Boundary Elements Method

The *Boundary Element Method*, a numerical discretization of the boundary integral formulation derived also from FEM formulation but, instead of modelling the whole volume takes only the boundary into account, while the inside of the object is physically modeled as an incompressible gas. The main difference is that BEM

considers only the elements on the surface of the volume, hence, the material properties should be defined uniform through all the object. The major drawback is the fact it can not handle internal multiple tissue models. BEM solves for forces and displacement on the boundary while FEM solves over the whole volume. In virtual surgery where interior forces and tissue characteristics affect the boundary, stress and internal deformations can not be ignored, FEM is still the right solution.

3.2.2.2 M_3: Mass-Spring Method

The Mass-Spring method is physically based technique that has been widely and effectively used for modelling deformable objects with real-time capabilities. The Mass-Spring model could be seen as a particle system (see Section 3.2.2.3) with fixed topology. The studied body is represented as a finite number of nodes. Neighbour nodes are connected with springs that introduce repelling and attractive forces into the system, maintaining the overall shape and position. Masses are assigned to each particle and a set of springs are allocated to connect it. The major difference between FEM and Mass Springs models comes from their origins. Both models are discrete approximations of the resulting deformation, but FEM is an approximation of a continuum where the Mass-spring model is discrete from the beginning.

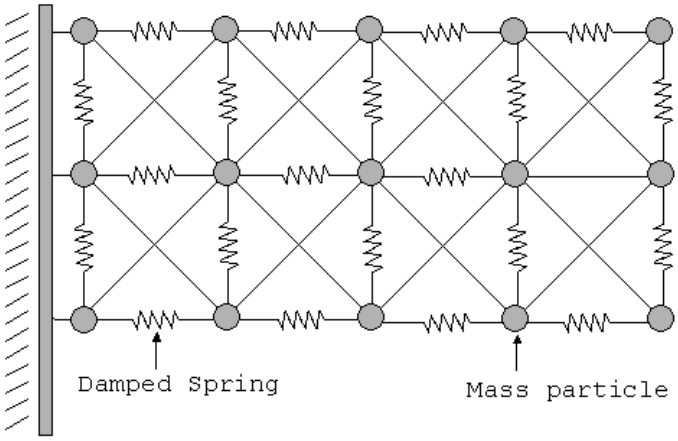

Figure 3.4: Example of Spring-Mass Model in which sixteen points mass are represented joined with spring connections with its neighbours. Diagonal connections are springs also.

As said earlier, a general mass-spring system consists of n mass points, each of

them being linked to its neighbours by massless springs of natural length greater than zero. Figure 3.4 shows an example of a Spring-Mass model. The nodes represent mass and inertia but have no volume. Each node of the system is governed by the basic Newton's law $f_i = ma_i$, where m is the mass of each point, a_i is the acceleration (or second derivative of the position) and f_i is the sum of all forces applied at point p_i. The force f_i can be divided into two categories: internal and external forces. The *internal forces* are due to the tensions of the springs. The overall internal force applied at the point p_i is a result of the stiffness of all springs linking this point to its neighbours. The *external forces* can differ in nature depending on what type of simulation we wish to model. The most frequent ones are gravity and viscous damping. The force added by each spring to the nodes that it connects is based on their distance. We have n nodes that approximate the shape of a volume Ω and $i, j \in \{1, 2...n\}$. Hence, at each node a more detailed equation of the Newton's law is given as,

$$f_i = m_i \frac{\partial p_i^2}{\partial t_i^2} + \gamma_i \frac{\partial p_i}{\partial t_i} - \sum_j g_{ij} \tag{3.11}$$

where m_i is the mass, γ_i the damping coefficient, and p_i the position of node i. The force $\sum_j g_{ij}$ is exerted on node i by the spring between nodes i and j. The physical behaviour of springs will determine the value of g_{ij}, thus, if it is considered as linear elasticity it can be set as $\sum_j k_{ij} p_i$ where k_{ij} is the stiffness coefficient corresponding to the spring that connects nodes i and j. The expression can be rewritten as a system of nodes. Being $p = (x, y, z) \in \Re^3$ the above expression of a single node can be added into one system of equations for all N nodes, where the unknown is a $3N \times 1$ vector p:

$$f = M \frac{\partial p_i^2}{\partial t_i^2} + C \frac{\partial p_i}{\partial t_i} + Kp \tag{3.12}$$

M and C are the $3N \times 3N$ diagonal mass and damping matrices corresponding to m_i and γ_i. The $3N \times 3N$ matrix K contains the spring stiffness coefficients between each pair of nodes, a zero value denotes no spring between them. This expression can be rewritten in terms of velocity and his first derivative as follows,

$$\begin{aligned} \frac{\partial v}{\partial t} &= M^{-1}(f - Cv - Kp) \\ \frac{\partial p_i}{\partial t} &= v \end{aligned} \tag{3.13}$$

Here we can observe how pre-computation can be applied to the inverse of the M matrix in order to achieve a faster computation. To simulate the system we should take small time-step, calculating using:

$$\begin{aligned} x_{t+1} &= x_t + \frac{\partial}{\partial x_i}\Delta t \\ v_{t+1} &= v_t + \frac{\partial}{\partial v_i}\Delta t \end{aligned} \tag{3.14}$$

Mass-Spring methods are easy to build and although simulation accuracy levels are not as high as those for FEM, its computational cost is relatively easy to improve using parallel processing. Despite of the advantages, mass spring models have drawbacks. The most important is that they only approximate the true physics of the continuous body and that spring constants are not always easy to estimate, producing inaccurate approximation of the physical behaviour of the material. Another problem is referred to as *stiffness*. When the spring constants are high, this causes instabilities in the system and produces slow simulations.

One of the first applications of the Spring-Mass models was the work of Provot *et al.* [106] for animating cloth objects. It has been widely applied in works on real-time simulation such as surgery training. A Mass Spring method was also used in the EyeSi simulator by Wagner *et al.* [142], a simulator for intraocular surgery. A common surgery procedure is to lift the retina by injecting salt solution beneath it. This procedure was modeled by treating the retina as a mass-spring mesh.

3.2.2.3 M_4: Particle Systems

Particle systems consist of a large number of point masses that interact with each other. Their movement is governed by the laws of physics (ie. external forces such as gravity or collisions). Each particle has a position, velocity, acceleration, mass, etc. The forces generated between particles and the environment is usually modeled with potentials and the movement of the particles follow Newtonian laws. Particle systems were originally used to model manifold physics phenomena including

galaxies, magnetic fields, compressible gases or explosions [109]. Particle systems have been used also to model deformable surfaces as description of cloth draping behaviour done by Breen [18].

Particle systems could not be clearly regarded as a shape/volume modelling technique. However various authors use this system for modelling. For instance in [139]. Tonnesen propose his "Oriented Particle System" where the surface representation is a triangulation mesh interpolating the particle position and direction. For deformable objects modelling, this model has to be improved by the introduction of internal forces between particles to preserve the cohesion of the object and characterise the internal volume. His system lacks of stability which is solved introducing damping forces. In [65] an interesting model where various layers with different elastic behaviours are modeled using particles system. The inclusion of a skeleton inside the particle system in [2] preserves the shape during the simulation and prevents the spherical tend of the system.

3.2.2.4 M_5: Finite Automata Methods

All these approaches deal with deformations computing simple calculations on a very large number of elements [49, 130]. *Chainmail* is perhaps the most common approach belonging to the set of techniques based on the *voxel* representation of the volume. Firstly introduced by Gibson *et al* [49] in a knee arthroscopy simulator, the Chainmail approach proposes a modelling methodology with no reduction in the resolution of the original data. In one dimension modelling, each element is connected to its two neighbours, as shown in Figure 3.5.

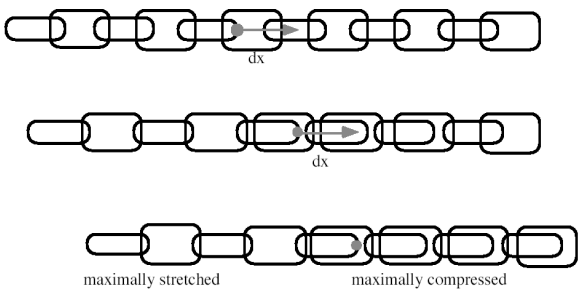

Figure 3.5: Deformation of a 1-D chain when the selected link is moved to the right by dx (from [49]).

In two dimensions (Figure 3.6) the neighbourhood grows to four elements. While in volume modelling (three dimensions) using Chainmail, each element is connected to six of its neighbours. These are top, bottom, right, left, front, and back. When the object is manipulated, each element is tested to see if it violates certain distance thresholds it shares with its neighbours. If the distances are reached, the element is moved in the corresponding direction. Else the object does not move. These rules are applied to the element, which are within the influence of manipulation and then propagates as a wave to their neighbours. Therefore, local deformations are generated only if distance thresholds are exceeded. Links between elements are initially set free, so movements only occur if the distances are violated. Elasticity or deformation constrains can be modeled by setting different distance values for different object types. For instance, small variations are given for rigid objects, while high values are specified for deformable objects.

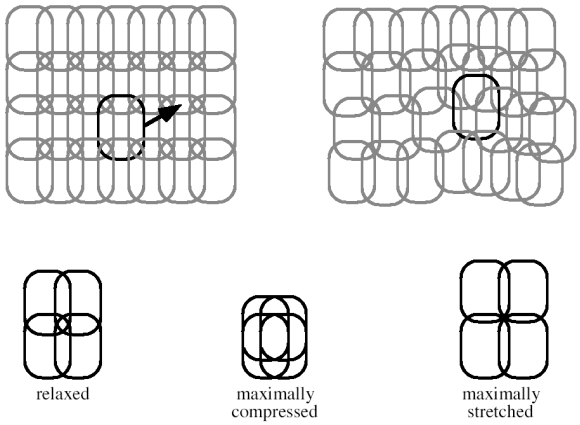

Figure 3.6: Deformation of a 2-D chain mail when the selected link (black) is moved (top row). Bottom row shows three typical Chainmail configurations.

This method allows to exploit all the resolution of the volumetric data generated by MRI or CT and applies simple calculations on elements to produce the deformation results. A range of material types can be modeled using this approach, such as rigid, deformable, plastic, and elastic [49]. The Chainmail method is also relatively easy to implement compared to other approaches. The *Sphere filled model* proposed by Suzuki *et al.* [130] is another example of an approach based on the sample principle.

3.2.2.5 M_5: Adaptive Methods

Many approaches have been presented to fill the gap between the accurate FEM methods and the fast but less accurate Spring-mass models. Conventional FEM is not real time, but some attempts have been presented to solve this problem. Adaptive meshing is necessary to provide sufficient detail where required while minimizing unnecessary computation as depicted in Figure 3.7. Zhuang *et al.* [155] introduces the use of a graded mesh instead of a uniform mesh, which reduces the complexity of a 3-D problem to a 2-D problem. Another example is found in Wu *et al.* [150] where authors apply nonlinear FEM using mass lumping to produce a diagonal mass matrix that allows real time computation.

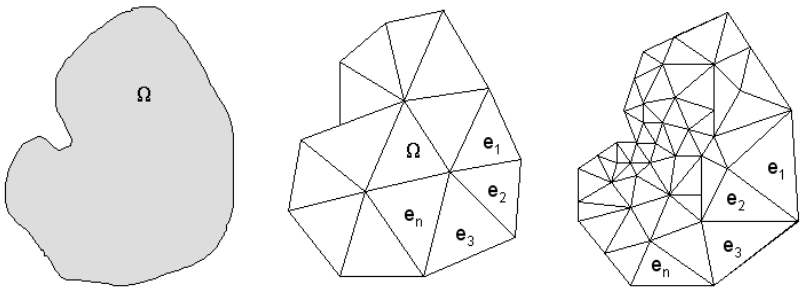

(a) (b) (c)

Figure 3.7: Discretization of the share Ω (a) into triangle elements using classic (b) and adaptive meshing (c).

Particle Systems and Mass-spring models are easily combinable as shown by Jaillet *et al.* [65] who proposed an adaptive structure that combined layers of particles with layers of mass-spring model as shown in Figure 3.8.

An adaptive method for animating dynamic visco-elastic deformable objects was proposed by Debunne *et al.* [34]. They use an automatic space and time adaptive level of detail technique, in combination with a large-displacement (know as Green) strain tensor formulation. The body is hierarchically partitioned into a number of tetrahedral regions and mass samples. The local resolution is determined by a quality condition that indicates where and when the resolution is too coarse. As the object moves and deforms, the sampling is refined to concentrate the computational load into the regions that deform the most. The model consists of a continuous equation solved using a local explicit finite element method. In Debunne's experiments,

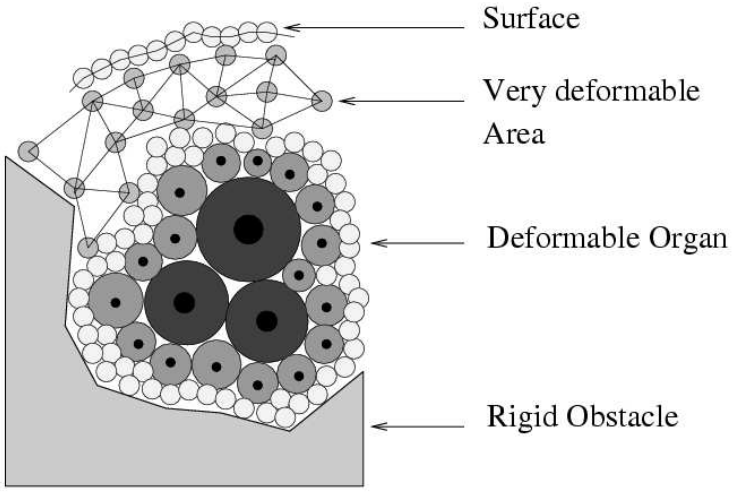

Figure 3.8: Sample of Particle Systems and Mass-spring combination model (reprinted from [65]).

movements exerted by the use of a haptic device are transmitted to the model, that deforms its shape and returns a response to the user through the the haptic device. The user has a realistic resistance response of the force exerted.

Instead of refining elements, Grinspun *et al.* [51] approach is based on the refinement of the basis functions, not the elements. This removes a number of implementation headaches associated with other approaches and becomes a general technique independent of dimension domain, element type (e.g. triangle, quadrangle, tetrahedron, hexahedron), and basis function order (piecewise linear, higher order B-splines, etc.).

Long Elements Method (LEM) [29] proposes a meshing based on long elements and the combination of elastic and static approaches to simulate the object. The Long Elements could be seen as an elastic spring, with a geometry of a deformable rod. It has defined its length and the area of its cross-section. This kind of meshing reduces the number of elements used to model the object and can easily handle large deformations over the object. The *Radial Elements Method* (REM) [7] is an evolution of some concepts introduced in the LEM approach. REM meshing is based on spherical geometry (radial elements). Both the LEM and REM are based on a static solution for elastic deformations of objects filled with uncompressible fluid. Each element has defined an equilibrium equation using volume variables.

The set of static variables plus the incorporation of the Pascal principle and the volume conservation are used to define a system that is solved to find the object deformation and forces, which are integrated to simulate movement.

3.3 Conclusions

This Chapter has presented the most commonly used techniques for deformation modelling. Different approaches have been described taken their accuracy an computation time into account as their most important characteristics. It has been shown that Geometric Models although less computationally costly are the less accurate. On the other hand, FEM based methods present the higher accuracy but pay an important charge related to its computation. Therefore, and thinking of applying deformable objects in a real-time environment as is the aim of this research a way forward is to use simplifications of FE Models such as BEM or other simpler models like Spring-Mass or Particle Systems. Undoubtedly, the accuracy of the models used is of vital importance in medical applications, therefore evaluation of the model is of paramount importance in this work and will be a focus of research on this thesis.

Figure 3.9 plots all reviewed deformation models against their estimated accuracy and computation time. FEM methods (as stated earlier) achieve the best accuracy, followed by simplifications of it such as LEM/REM and adaptive systems. Particle Systems and Spring-Mass methods present a good tradeoff between accuracy and cost, which should be further examined in this thesis to assess if it can be used for accurate breast modelling and surgical applications.

Summarising, Table 3.1 shows various published works on deformable models classified by the technique used. It should be noted that the table shows main and representative works but not an extensive list of all published works on deformable models. In addition, deformable models applied to breast images are shown in bold in the table. One can notice that modelling methods applied on breast modelling are mainly represented by FEM. The next Chapter comes motivated from the need of modelling internal breast tissue distribution. Hence, a feature extraction process is needed to know the nature and tissue distribution. Next Chapter will be focused on feature extraction in X-ray and MR images.

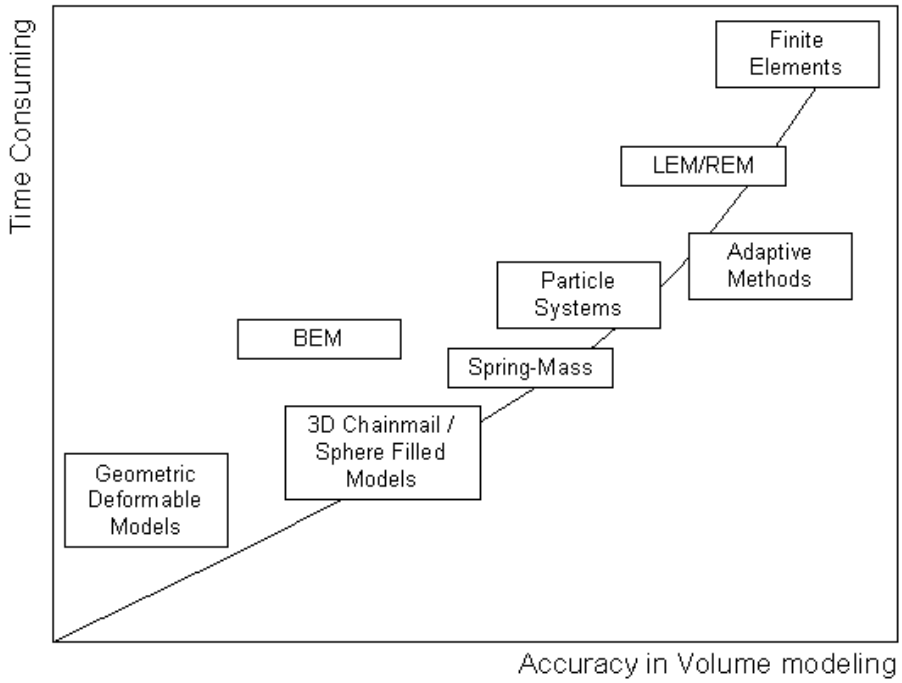

Figure 3.9: Deformable volume modelling performance estimations.

Methods	**1980's**	**1990's**	**2000's**
Geometric Deformable Models	Barr84 [8] Sederberg86 [122] Bookstein89 [15]	Sabine90 [28] William92 [61] Singh98 [125]	Schnabel01 [119]
Particle Systems	Reeves83 [109]	Szeliski92 [132] Tonnesen98 [139]	Amrani00 [3] Baudet03 [10]
Finite Elements Method	Platt88 [104] Cotin98 [30]	Terzopoulos89 [138] Keeve96 [72] Bro-Nielsen96 [19]	**Azar00 [5]** **Samani01 [116]** **Tanner01 [135]** **Sciarretta02 [121]** **Schnabel03 [120]** **Galea03 [46]** Liu03 [83] **Qiu04** [108] **Ruiter04 [113]**
Boundary Elements Methods		James99 [67]	Hui02 [62]
Spring-Mass Models		Provot95 [106] Kita96 [74] Christensen97 [25] Nedel98 [98]	Wagner02 [142] Anderson03 [4] **Roose05 [111]**
Finite Automata		Gibson97 [49]	Li03 [82] Suzuki04 [130]
Adaptive Approaches	Yserentant86 [153]	Zhuang99 [155]	Debunne00 [33] Wu01 [150] Grinspun02 [51] Balaniuk03 [7] Hauth04 [54]

Table 3.1: Classification of deformable modelling proposals.

Chapter 4

Mammographic Feature Extraction

The previous Chapter has shown how significant is modelling the whole volume, boundary and internal layers. In breast modelling, knowledge of internal tissue is needed to correctly model its compressible nature. This Chapter presents various mammographic feature extraction approaches, mainly related to the profile and tissue characterisation from the X-ray mammography and MR volume, which will be needed to correctly integrate both modalities in our model.

4.1 Introduction

The biomechanical modelling of biological structures requires a knowledge of the geometrical model and the mechanical properties associated to each tissue. Having the breast modelling challenge in mind, the contribution of X-ray mammography and MR data involves some feature extraction processes in order to obtain the breast profile and correctly characterise tissue properties from both modalities. This measures enable an accurate breast geometry modelling and a realistic estimation of tissue elastic properties without *in-vivo* measurements.

Figure 4.1 shows the appearance of the breast, viewed trough the two main modalities, X-ray and MR Imaging. In X-ray mammograms, ducts and lobules are usually represented in various bright grey scale densities, while fatty tissue, is imaged

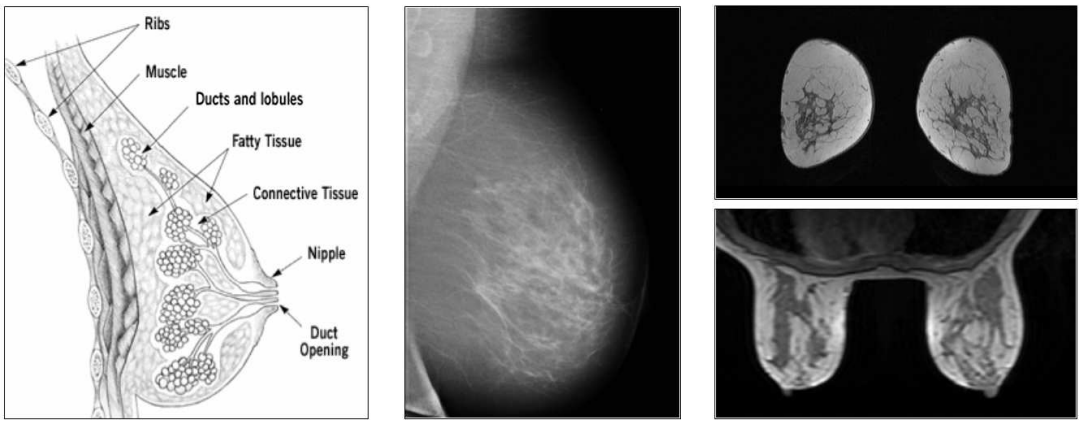

(a) (b) (c)

Figure 4.1: The tissue appearance relationship between (a) the schematic view of breast anatomy and the samples of (b) X-ray mammogram and (c) two MR slices; top image, sagittal view and transversal view in the bottom.

as nearly transparent regions (dark grey scale values). The pectoral muscle usually is represented in MLO views as the brightest region having a triangular shape. Lesions are represented as bright areas equal or brighter than parenchymal tissue, hence the difficulty to detect lesions in dense mammograms. In the case of MR slices, ducts and lobules (parenchymal tissue) are depicted as a mass of homogeneous densities in the middle range of the grey value scale. The fatty and the connective tissue are represented by bright grey values. Although the skin has the same grey value intensities as the parenchyma it should be differentiated by its position outside the breast area. In order to enhance abnormality signs, contrast agents are commonly used in MR imaging.

Feature extraction plays an important role as a first step for building an accurate deformable model. This Chapter reviews various approaches for feature extraction (breast segmentation, tissue classification) applied to X-ray and MR mammographic modalities.

4.2 Breast Profile Segmentation in X-ray Imaging

The automatic breast segmentation into background and breast regions removing artifacts (directly exposed area, the patient identification information and lead mark-

ers), is a key objective to provide useful data to the computerised analysis. Figure 4.2 shows an example of breast profile segmentation. Previous works on breast tissue identification and abnormality detection notice that the feature extraction process is affected if the region processed is not correctly extracted. Thereby, it is important to split the mammogram into interesting regions to achieve optimal breast parenchyma measurements, as an initial step for breast registration or to select the region of interest where abnormalities could be found. In the following section, most of the relevant work that has been presented from 80's to nowadays is under review.

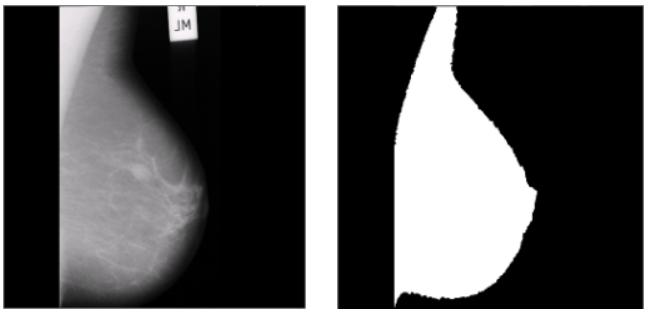

(a) (b)

Figure 4.2: (a) X-ray mammogram and (b) breast profile segmentation.

Breast gross-segmentation has been widely treated. Table 4.1 shows the tendencies and distribution of methods from the firsts works to recent approaches. The remaining of this section will review some of these techniques following this classification: Histogram, Gradient, Polynomial Modelling and Classifier approaches.

- ***Histogram based techniques.*** Probably one of the first attempts to separate the breast region was presented by Hoyer *et al.* [60] in 1979, and it was done using simple histogram thresholding. In a similar way the works of Lau *et al.* [80], as well as Yin *et al.* [152], and Byng *et al.* [21] used a simple thresholding to segment the breast from the background. The work of Bick *et al.* [13] presented a combination of local thresholding, region growing and morphological filtering. Hein *et al.* [55] proposed their own global histogram thresholding, while Masek *et al.* [92] proposed a local thresholding method in 2000.

- ***Gradient based techniques.*** Breast region extraction techniques based on gradient have long been in use, since the early work of Semmlow *et al.* [123]

Methods	1980's	1990's	2000's
Histogram	Hoyer79 [60]	Lau91 [80] Yin91 [152] Bick95 [13] Byng96 [21] Hein98 [55]	Masek00 [92]
Gradient	Semmlow80 [123]	Méndez96 [94] Abdel-Mottaleb96 [1] Morton96 [97] Karssemeijer98 [71]	Zhou01 [154]
Polynomial Modelling		Stomatakis94 [127] Chandrasekhar96 [23] Goodsitt98 [50]	
Active Contours		Ojala99 [101]	Ferrari00 [43] McLoughlin00 [93] Wirth04 [148]
Classifiers			Saha01 [115] Rickard03 [110] Wirth04 [147] Tromans04 [140]

Table 4.1: Classification of breast gross-segmentation proposals.

in 1980, who by means of spatial filters and a Sobel edge detector obtains the breast boundary. Similarly, Méndez *et al.* [94] use a two-level histogram threshold to obtain the breast region, the region is then divided into three parts to track the boundary using the gradient information. An evaluation of the quality of the segmentation is provided using the "accurate" or "near accurate" labels. They successfully compare their results with the work presented by Yin *et al.* [152]. The work presented by Karssemeijer *et al.* [71] takes advantage of a multiresolution scheme, processing in low resolution and extrapolating the result. Using a global thresholding technique they obtain a preliminary region, which is processed using a 3x3 Sobel operator, while the pectoral muscle position is estimated via Hough transform. Abdel-Mottaleb *et al.* [1] provide an scheme based on different thresholds to find the breast edge. Using the gradient of two images and its union they obtain a possible breast contour. They found the boundary in 98% of the 500 images tested. The segmentation presented by Morton *et al.* [97] was another gradient based method. After subtracting the background via an initial threshold, an edge was found by a line-by-line gradient analysis. Zhou *et al.* [154] presented an improvement of this last approach in 2001.

- ***Polynomial Modelling based techniques.*** An early method proposed by Stomatakis *et al.* [127] in 1994 was not a strict polynomial modelling. By

means of an image preprocessing technique to enhance the response of non-dark pixels, a noise reduction process and a histogram threshold, they obtain the breast region, but the boundary is smoothed using Cubic B-splines and samples at fixed pixel intervals are extracted. Then a smooth curve is generated through cubic polynomial calculations. One of the firsts, effective and real polynomial modelling was presented by Chandrasekhar and Attikiouzel [23]. An initial threshold is used to approximate the breast region. Their method provides around 94% acceptable results from 300 images from MIAS [63] mammogram database. A quadratic/cubic polynomial fitting method was proposed in 1998 by Goodsitt *et al.* [50] which was fitted by a translation and rotation of the axes.

- ***Active Contours based techniques.*** These techniques can be seen as enhanced evolution of the gradient approaches. One of the firsts applications of the active contours on breast segmentation was presented in 1999 by Ojala *et al.* [101]. McLoughlin *et al.* [93] applied a global threshold to obtain an initial result. They statistically model the breast with the pixels inside the region and a snake algorithm is applied to obtain the final boundary. On the other hand, Ferrari *et al.* [43] proposed a method that firstly enhances the image with a logarithmic transformation, and then an iterative technique (as the Lloyd-Max least-squares [84]) is applied to find an optimal threshold. Finally, they use a B-Spline to approximate the boundary. Recently, Wirth *et al.* [148] proposed in 2004 an active contour to segment the breast. The method obtains two preliminary regions using a convolution matrix to enhance the edges and a dual threshold obtained by different techniques. They obtain the control points for the snake by comparing both regions and evaluate the method over the MIAS database.

- ***Classifiers based techniques.*** Saha *et al.* [115] used a scale-based fuzzy connectedness algorithm in 2001. Rickard *et al.* [110] presents Self-organizing map, a type of unsupervised artificial neural network model to segment the breast. The method applied by Wirth *et al.* [147] was a fuzzy segmentation approach evaluated in terms of completeness and correctness comparing the images from the MIAS database with a gold standard manually generated. Recently, Tromans *et al.* [140] in 2004, use a mixture model to obtain a mathematical representation of the image background and the compressed para-

meters, combined with a Fourier model, using an Expectation Maximization algorithm.

In summary, a traditional histogram based method has provided good and quick results (see our propose in Chapter 5). This quality sometimes turns to a weakness in difficult cases where results can be enhanced with local histogram or gradient approaches. The polynomial modelling and active contours provide very good results with accurate profiles, paying a higher computational cost.

4.3 Tissue Classification

Recent studies have shown that the sensitivity of Computer Aided Diagnosis (CAD) systems is significantly decreased as the density of the breast is increased while the specificity of the systems remained relatively constant [59]. The origins of breast density classification are the work of Wolfe [149], who showed the relation between mammographic parenchymal patterns and the risk of developing breast cancer, classifying the parenchymal patterns in four categories. Since the discovery of this relationship, automated parenchymal pattern classification has been investigated. In addition, and within the scope of this research, tissue classification is of great importance as can be used for understanding tissue mechanic characteristics and this information, incorporated when building the breast deformation model.

4.3.1 Breast tissue in X-Ray images

It is well known that information derived from mammographic parenchyma patterns provides one of the most robust signs of risk of developing breast cancer. The American College of Radiology (ACR) Breast Imaging Reporting and Data System (BIRADS) [100] is becoming a standard on the assessment of mammographic images. Breast density is classified in four categories as shown in Table 4.2.

Once the breast profile is extracted using a segmentation algorithm as explained in Section 4.2 we proceed to classify the breast tissue. We have found in the literature different approaches for classifying the breast tissue based only on the use of histogram information [154]. However, histogram information seems to be not sufficient to classify a mammogram into BIRADS categories. For instance, second row

BIRADS Number	Findings
I	the breast is almost entirely fatty.
II	there is some fibrogandular tissue.
III	the breast is heterogeneously dense.
IV	the breast is extremely dense.

Table 4.2: Breast density BIRADS categories.

of Figure 4.3 shows the histograms for four different mammograms, each belonging to a different class. As we can see, it seems difficult to think that they belong to different classes. For resolving this kind of ambiguities, texture analysis can be is applied.

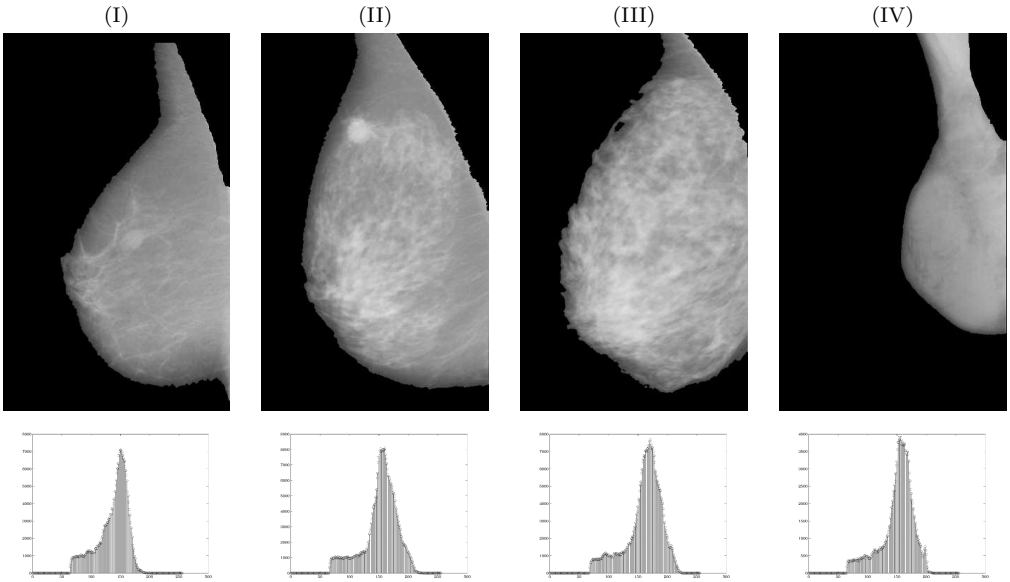

Figure 4.3: Four similar histograms, each of increasing BIRADS category: from (a) BIRADS I to (d) BIRADS IV.

Typical grey-level approaches consist on computing the histogram of the breast with the aim to find the best threshold to segment the mammogram. As a result of this procedure, regions with fatty tissue are segmented from regions with dense tissue [17, 115, 126]. Thus, according to the relation of both classes they can determine to which class the breast is classified. Zhou *et al.* [154] modified this strategy in order to take advantage of the a priori information: instead of using a unique

threshold for segmenting all the mammograms, they first classify them into four different classes according the histogram behaviour, and then, they segment using different strategies for each class. On the other hand, Karssemeijer [71] noted that the appearance of the mammographic tissue is influenced by the variation of tissue thickness in the periphery of the breast. This is plausible, as the breast is compressed in between two stiff plates during the imaging procedure, and the periphery of the breast is composed mainly of fat tissue which is very flexible. In this way, its proposal was to divide the breast on different regions according to the distance among the pixels and the skin line. Following, according to different grey-level based features, he classified the breast into different classes.

On the other hand, different papers have suggested that texture representation of the breast might play a significant role. Miller and Astley [95] investigated texture-based discrimination between fatty and dense breast types applying granulometric techniques and Laws texture masks. The works of Caldwell *et al.* [22] and Byng *et al.* [21] were based on measures extracted from fractal dimension. Bovis and Singh [16] estimated features from the construction of Spatial Grey-Level Dependency matrices. Recently, Petroudi *et al.* [102] used *textons* to capture the mammographic appearance within the breast area. Zwiggelaar *et al.* [157] segment mammograms into density regions based on a set of co-occurrence matrices. Density classification uses the size of the density regions as the feature space. This work was extended in [158] were a transportation algorithm was used to select an *optimal* set of co-occurrence matrices for the segmentation process.

Features	**1990's**	**2000's**
Histogram	Hajnal93 [52] Boyd95 [17] Tahoces95 [134] Highnam96 [57] Karssemeijer98 [71]	Saha01 [115] Sivaramakrishna01 [126] Zhou01 [154] Marias02 [89]
Texture	Caldwell90 [22] Miller92 [95] Suckling95 [128] Byng96 [21]	Blot01 [14] Bovis02 [16] Petroudi03 [102] Zwiggelaar03 [157] Zwiggelaar04 [158]

Table 4.3: Classification of breast tissue classification proposals.

Table 4.3 shows the related works arranged by proposal's decade and the features used to classify the breasts. Note that although the first works of classification were based on texture features, most of the earlier works were based only on grey-level

information. The most recent works could change this trend and texture representations will be more popular than just using grey-level information.

4.3.2 Breast tissue in MR images

Much more efforts have been dedicated to tissue classification in X-ray mammograms compared to MRI. Perhaps, due to fact that the signs shown in MRI are not as crucial as the ones shown in X-ray mammograms. Basically, three main regions can be observed in a MR breast image: background, fatty and glandular tissue (as shown in the MR slice in Figure 4.4a and usually with well defined transitions between them. The knowledge of the tissue types and its distribution inside the breast is useful for volume estimation measures and model building. We should remember that MR imaging is the most realistic representation of the uncompressed breast that we have, thus it is a very good base to build a model.

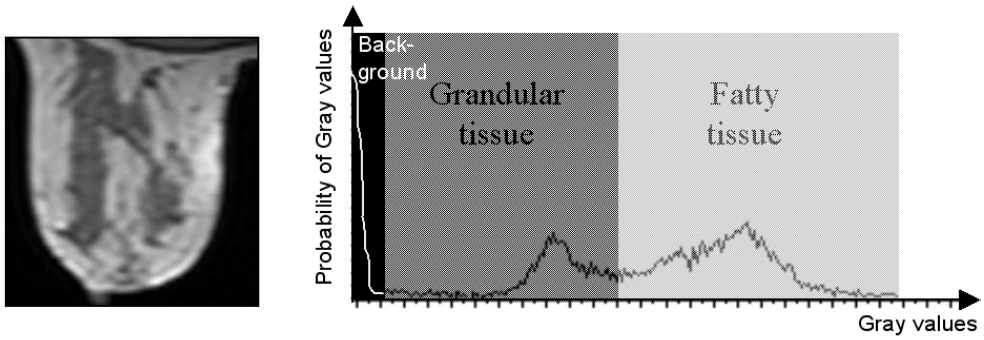

(a) (b)

Figure 4.4: An example of MRI histogram.(a) Original MRI slice, (b) Histogram.

In order to build a model based on MR data, an initial segmentation of the 3D volume is required to quantify the tissue distribution. The most accurate way to classify the tissue is the manual classification done by an expert. A major drawback of manually segmenting the internal structures is that involves an interaction from the user. Specially the classification of the transition regions is a long and tedious work based on subjective judgements, which does not have a good clinical approval. As can be seen in Figure 4.4b the grey levels histogram distribution of each tissue type are easily separable. Usually thresholding approaches are used due to reduces the expertise load, which only should to select the adequate threshold values.

As well as manual segmentation or thresholding approaches, methods like region growing [44], clustering, and probabilistic methods could be used to classify the tissue type from MRI. This algorithms are widely used in generic segmentation. Two major problems should be noticed: 1) the user usually has to select the initial number of seeds and, 2) the final partition could be a local solution, that is, there could be another partition of the image that is a better approach to the human vision. This second problem is also referred to as the problem that different seed location involves different final solutions.

These drawbacks do not affect the case of tissue segmentation because an unsupervised segmentation algorithm is used and the number of partitions we look for is known. In that sense, typical clustering algorithms for image segmentation such as k-Means (KM) [66], Fuzzy C-Means (FCM) [12] and the Expectation-Maximization algorithm (EM) [37], provide very good results due to its partitional nature of the image into a number of regions known. The performance of these algorithms has been deeply studied and compared [66]. Following, we briefly review these methods.

- **K-Means Algorithm** The popular k-Means algorithm, first proposed by [86], is an error minimization algorithm where the function to minimise is the sum of squared error:

$$e^2(K) = \sum_{k=1}^{K} \sum_{i \in C_k} ||x_i - c_k||^2 \tag{4.1}$$

  where c_k is the centroid of cluster C_k. Two factors had made the k-Means one of the most popular clustering algorithms: it has linear time complexity and it is easy to implement [66].

- **Fuzzy C-Means Algorithm** The k-Means algorithm associates each pattern of the image to one and only one cluster. With the use of the fuzzy theory, each pattern can be associated with every cluster using a membership function. The error minimization function is defined as:

$$e^2(\Xi, U) = \sum_{k=1}^{K} \sum_{i=1}^{N} u_{ik} ||x_i - c_k||^2 \tag{4.2}$$

  where Ξ is the partition of the image, U is the membership matrix: u_{ik} represents the membership of pattern x_i to belong to cluster k, which have center

$c_k = \sum_{i=1}^{N} u_{ik} x_i$, N is the number of patterns of the image (number of pixels), and K the number of clusters, which have to be known a priori. The reader is referred to the book of Bezdek [12] for the basics of this algorithm.

- **EM Algorithm** Another way to assign each pattern to belong to a specific cluster is the Gaussian Mixture model. In this probabilistic model, each pattern is characterised by a set of Gaussian mixtures:

$$p(x_i; K) = \sum_{k=1}^{K} \pi_k g_k(x_i) \tag{4.3}$$

where g_k is a Gaussian distribution and π_k a prior distribution ($\sum_k \pi_k = 1$). The model parameters and cluster membership are determined by maximizing the log-likelihood estimator:

$$l(K) = \sum_i log(p(x_i; K)) \tag{4.4}$$

This second step is efficiently done using the Expectation Maximization algorithm [37].

4.4 Conclusions

This Chapter has presented feature extraction as a pre-processing step for building a breast correspondence model. Basically, information about the extraction of the profile and tissue type from X-ray mammograms and MR images has been presented.

Reviewed works on breast profile segmentation have shown a wide spectrum of approaches. One should notice that the high image quality provided by new Full Field Digital Mammograms (FFDM) allow clear-cut breast profile, which does not happen in digitised mammograms. This fact has an important relevance as simple and fast approaches using FFDM provide similar results compared to the ones obtained with more complex methods.

There are several approaches of breast tissue classification in X-ray mammograms which characterise tissue distribution for risk assessing purposes. Histogram and texture information in which the main works are based, generally show good results.

In this work tissue information is of crucial importance to correctly characterise our model. Although there is not an extensive literature on tissue classification using MR images, it has an important role in breast modelling. MR data provides useful information to correctly characterise breast tissue and breast geometry. Tissue identification jointly with *in-vivo* measurements of mechanical tissue behaviours enable the realistic modelling the soft tissue mechanics.

In the next Chapter our firsts steps towards the breast model building are explained. From the breast profile estimated using X-ray mammograms to tissue characterization extracted from X-ray and MR imaging.

Chapter 5

Realistic Correspondence Model for Multi-modality Mammography

Once reviewed the main approaches on mammographic correspondence, modelling techniques and internal tissue characterisation, initial steps toward building our breast model and results are presented in this Chapter. Novel approaches for mammographic feature extraction are discussed and evaluated, specially focused on breast profile segmentation and breast tissue classification. Those results are subsequently used for building an initial breast surface model.

5.1 Introduction

The prerequisite for the adequate simulation of soft tissue deformations is the correct conversion of the anatomy into a geometrical model. The final goal of the breast model should be to account for internal tissue deformation as realistic as possible.

In this Chapter, we describe the major steps needed to create a useful volumetric model of the breast's anatomy using MR data. Firstly we propose an automated method to segment the digital mammogram into breast region and background with a new pectoral muscle suppression technique. Breast profile from X-ray mammograms can be used as boundary constraint for the deformable model. In addition, the mesh that represents the breast is extracted from the segmented MRI (Section 5.3) where tissue types are classified into fatty and glandular tissue (Section 5.4).

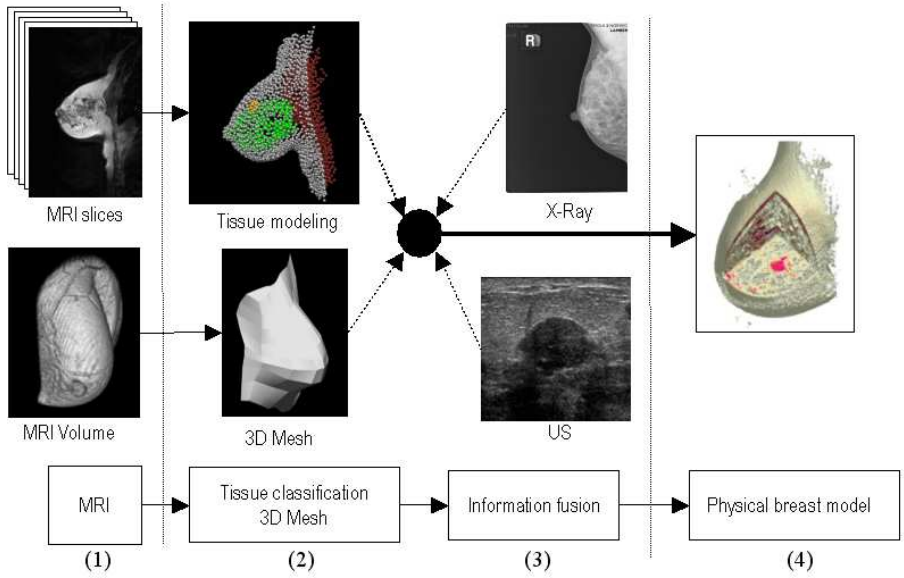

Figure 5.1: Model building process. Last right image taken from [146]

Figure 5.1 depicts a global scheme of our final goal: The building of a realistic correspondence model to multi-modality mammography. Realistic breast model building follows some steps: starting with a breast geometry extraction process from MR imaging, following with the tissue elastic properties modelling and finally integrating both information into a physical breast model. Each modality, X-ray and MR imaging will provide features that should be carefully taken into account. Next sections present our contribution to model building.

5.2 Breast Profile Segmentation

To obtain the breast profile segmentation using X-ray mammograms we propose a "two-phase" based method. It combines an adaptive histogram approach to separate the breast from the background (Phase A), and a selective region growing algorithm to obtain pectoral muscle suppression (Phase B). Figure 5.2 shows a visual scheme of the proposed method.

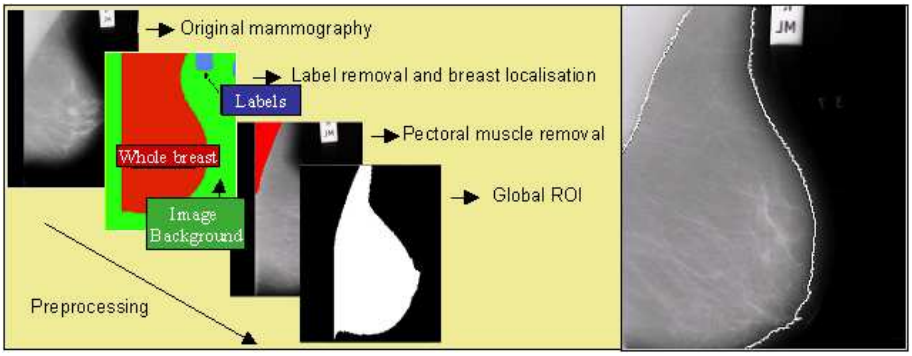

Figure 5.2: Global Segmentation. Breast region extraction and pectoral muscle suppression.

5.2.1 *Phase A*. Breast Segmentation

The aim of Phase A is to obtain a breast mask removing non-desirable image artifacts (labels, patient information, etc). Figure 5.2 shows the steps followed from the original mammogram to obtain the breast mask. A global histogram is calculated and smoothed with a Gaussian operator. Subsequently, N consecutive percentage of bright pixels are tested to obtain N thresholds (ie. 10%, 15%, 20% that in grey level means 220, 210, 200). Each value is used in order to threshold the image and obtain masks which are overlapped. The region defined by the boundary of the smallest threshold to the boundary of the largest one is statistically evaluated to calculate the mean of the grey level which is used as our final threshold value. The result of applying this threshold is a collection of different regions. The largest one is the union of the breast and the pectoral muscle. We extract this largest region using a Connected Component Labelling algorithm [118]. In Figure 5.2, the region of interest of the breast has been extracted from the pectoral muscle using the region growing algorithm described above. In the following section we introduce a new method to detect the pectoral muscle using a selective region growing approach.

5.2.2 *Phase B*. Extracting the Pectoral Muscle

This operation is important in mediolateral oblique views (MLO), where the pectoral muscle, slightly brighter compared to the rest of the breast tissue, can appear in the mammogram.

Previous work related to pectoral muscle suppression used Hough Transform [71, 78], assuming that the boundary between the pectoral muscle and the breast can be approximated by a straight line. Other related work is by Yam *et al.* [151] whose work introduces a curvature component to the Hough estimation and the work presented by Ferrari *et al.* [42] who propose a polynomial modelling of the pectoral muscle. The method we propose is inspired in the proposal of Georgsson [48] and it follows three steps:

I. **Breast localisation and orientation**. To classify the mammogram as right or left breast, we compare both sides of the breast profile, and using the curvature detected in each one, it is straightforward to determine the orientation.

II. **Region growing intensity threshold estimation (RG)**. Once the orientation is known, a seed is placed inside the pectoral muscle (the first pixel of the non-curved side). A statistical region growing algorithm (RG) grows from this seed to fill the whole region of the pectoral muscle. A size restriction has been applied to avoid an incorrect growing. When the limit of growing is exceeded, the growing criteria is corrected. This correction is estimated from the histogram of the previous region grown, progressively decreasing the initial value of the growing criteria. Then the RG is restarted as shown in Figure 5.3. If a correct growing is not found in finite steps, the initial mask is provided as a result and the no existence of pectoral muscle is assumed.

III. **Boundary refinement**. Finally, the pectoral muscle is suppressed from the breast region, and a round shaped morphological operator is applied to refine the boundary.

5.2.3 Experimental Results

We have used the public database MiniMIAS [129] to test our method. It is a reduced version of the original MIAS Database (digitised at 50 μm pixel size) that has been reduced to 200 μm pixel edge and clipped or padded so that every image is 1024x1024 pixels.

Figure 5.4 shows three representative results. We have tested over 322 images, and we have obtained a 98% of “near accurate“ results, which include the “accurate“

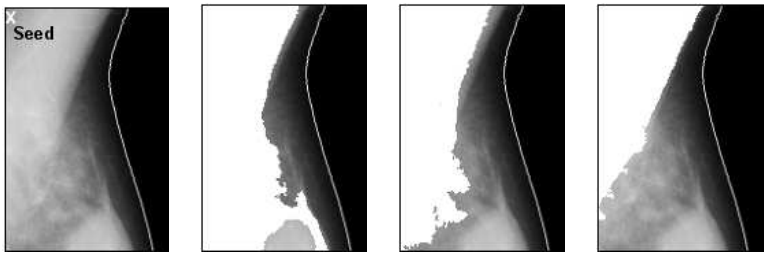

(a) (b) (c) (d)

Figure 5.3: Pectoral muscle removal. Region growing criteria correction. (a) original image,(b-c) incorrect growing (d) final correct RG.

results. About the muscle substraction, we have obtained a 86% of good extractions. Those results are obtained from a visual inspection of the images carried out by experienced radiologists and technicians trained with those kind of images. We should notice that some of them are a little bit over or under segmented. The behaviour of the method shows an over-segmentation of the breast in cases with dense tissue, where the contrast between the muscle and the tissue is fuzzy. In those cases, our method rejects the muscle detection and provides the region obtained without suppressing the muscle as a final result. A possible solution could be to impose shape restrictions to the growing process.

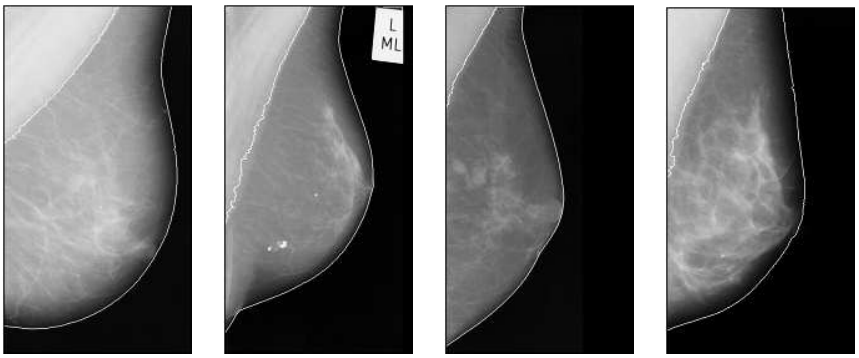

(a) (b) (c) (d)

Figure 5.4: An example of the performance of the presented approach on the segmentation of the profile of four different breasts.

To summarise, the results obtained by the method show that it is a robust approach but it can be improved in terms of accuracy. Even so, we accept this method because it provides useful regions (there is no meaningful loss of information). We

consider that is important to take some shape features into account to deal with the more accurate pectoral muscle suppression. The results have shown that problems with the image acquisition, background noise, artifacts and scratches could all influence the reliability of the algorithm.

5.3 Tissue Classification

Once the breast profile is detected on a X-ray mammogram, a step forward is to classify the breast tissue. Tissue distribution in each modality is useful for building the model, as provides valuable information about the elastic characteristics of breast which will be incorporated in the model.

The following sections present tissue classification solutions in both modalities, X-ray mammogram and MR images.

5.3.1 Tissue Classification in X-ray imaging

We consider that those pixels with similar internal tissue have similar grey-level values, as can be seen in Figure 4.3. We use the Fuzzy C-Means algorithm [12] to group pixels into separate categories (see Chapter 4 for a further explanation). However, to avoid effects from microtexture that could appear in some regions, we first smooth the breast region with a median filter of size 5×5.

Fuzzy C-Means is an extension of the well known k-Means algorithm. The main difference is that Fuzzy C-Means lets each pattern of the image to be associated with every cluster using a fuzzy membership function (in k-Means, each pattern belongs to one and only one cluster). When using partitional clustering algorithms, like Fuzzy C-Means, the placement of the initial seed points is one of the central issues in the variation of segmentation results. Despite their importance, usually seeds of these algorithms are initialised randomly. In our approach, the Fuzzy C-Means is initialised using histogram information, with the aim to obtain representative instances of two classes: normal and dense tissue. Hence, we initialise the two seeds with the grey level values that represent 15% and 85% of the accumulative histogram (of the breast pixels). Figure 5.5 illustrates the seed placement approach.

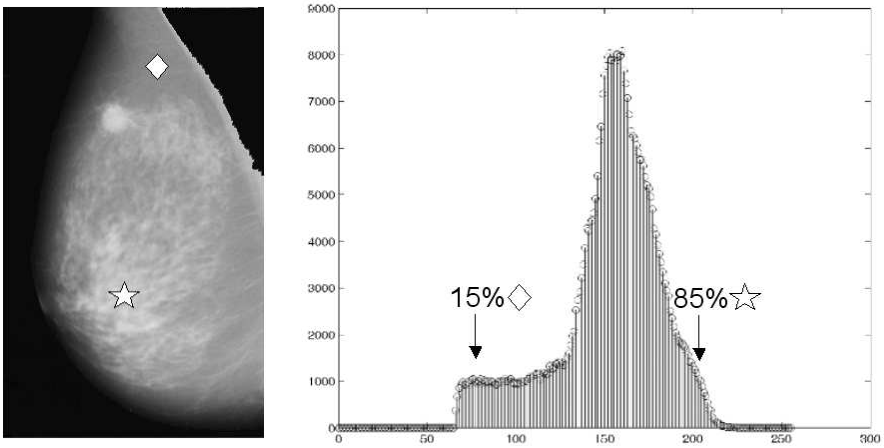

(a) (b)

Figure 5.5: An example of the Fuzzy C-Means seed placement where (a) shows the X-ray mammogram with the two seeds and (b) depicts the intensity values of this seeds, selected according to the given percentages.

5.3.1.1 Extracted Features

When Fuzzy C-Means finishes the breast is divided into two clusters. A set of features for each class can be directly extracted. We used a set of morphological and texture features. As morphological features we simply calculate the relative area, the center of masses and the mean intensity of both clusters, whilst as textures features, we calculate features derived from co-occurrence matrices [53].

Co-occurrence matrices are essentially two-dimensional histograms of the occurrence of pairs of grey-levels for a given displacement vector. Formally, the co-occurrence of grey levels can be specified as a matrix of relative frequencies P_{ij}, in which two pixels separated by a distance d and angle θ have gray levels i and j. Co-occurrence matrices are not generally used as features, rather a large number of textural features derived from the matrix have been proposed [53]. Here we use 4 different directions: 0°, 45°, 90°, and 135°; and a distance equal from 1 to 10. This distances have been chosen experimentally according to observed glandular tissue dimensions in our database. For each co-occurrence matrix we determine the contrast, energy, entropy, correlation, sum average, sum entropy, difference average, difference entropy, and homogeneity features.

5.3.1.2 Classification

We use the k-Nearest Neighbours classifier algorithm [86]. The k-Nearest Neighbours classifier [40] (kNN) consists of classifying a non-classified vector into the k most similar vectors found in the training set. Figure 5.6 illustrates the idea behind kNN where the unclassified vector is assigned to the proximity of its neighbours.

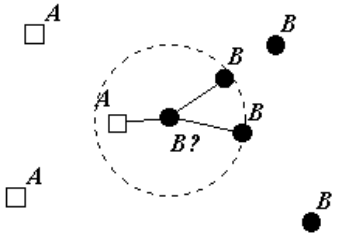

Figure 5.6: k-Nearest Neighbours rule.

Because kNN is based on distances between sample points in feature space, features need to be re-scaled to avoid that some features are weighted much more than others biasing the results. Hence, all features have been normalised to unit variance and zero mean. For the kNN classifier, the membership value of a class is different from zero if there is at least one neighbour (of k possible neighbours) belonging to this class. The membership value for each class will be the sum of the inverse Euclidean distances among each neighbour of the class and the pattern. A final unit normalisation between all the membership values is required.

5.3.1.3 Experimental Results

The method was applied on a set of 320 mammograms taken from the MIAS database [129]. This database is composed by the mediolateral oblique views of both breast of 160 women. The spatial resolution of the images is $50\mu m$ x $50\mu m$ and quantised to 8 bits.

The MIAS database provides ground truth tissue classification results that classifies the tissue as *Fatty* (106 images), *Glandular* (104 images) and *Dense* (112 images). In order to evaluate the method using this ground truth, we performed two experiments.

The first experiment was performed over the set of fatty and dense mammograms, and using only morphological features extracted from the segmented clusters. We calculated the relative area, the center of masses and the mean intensity of both clusters. These features are used as the input parameters for the classification stage. In order to evaluate the results, we use a leave-one-out method, in which each sample is analysed by a classifier which is trained using all other samples except for those from the same woman. The results showed that 87% of mammograms were correctly classified using the kNN classifier ($k = 7$). However, when including the glandular class, results were drastically decreased to 42%. This due to the fact that glandular breasts are more difficult to classify even by radiologists themselves and the use of morphological features alone does not present enough discriminant characteristics.

		Automatic Classification		
		Fatty	Glandular	Dense
Truth	Fatty	23	6	1
	Glandular	2	22	6
	Dense	1	14	15

Table 5.1: Confusion matrices of the kNN classifier.

The second experiment was performed using all the cases and using the morphological features cited above as well the texture features. The efficiency of the classifiers were computed using again the same leave-one-woman-out approach. Experimental results showed that classification results were improved when the cluster means were subtracted from the feature vectors. The reason for this can be found in the fact that increasing the dense area of the breast, results in a larger difference between the two tissue type clusters.

The confusion matrix for our classifier is shown in Table 5.1. A confusion matrix should be read as follows: rows indicate the object to recognise (the true class) and columns indicate the label the classifiers associates with this object. We can also note in Table 5.1 that mammograms belonging to a fatty and glandular class are better classified than the rest of mammograms when using the kNN approach.

5.3.2 Tissue Classification in MR imaging

In order to classify the breast tissue in MR imaging, we have used three typical clustering partitional algorithms, which are the k-Means, the Fuzzy C-Means and

the Expectation-Maximization algorithm, which have been briefly detailed in the previous Chapter (Section 4.3.2). Initial number of clusters has been set to classify the three main regions observed in a MR breast image: background, fatty and glandular tissue (parenchymal tissue).

Figure 5.7 shows examples of the classification results obtained over one MR slice using the three approaches.

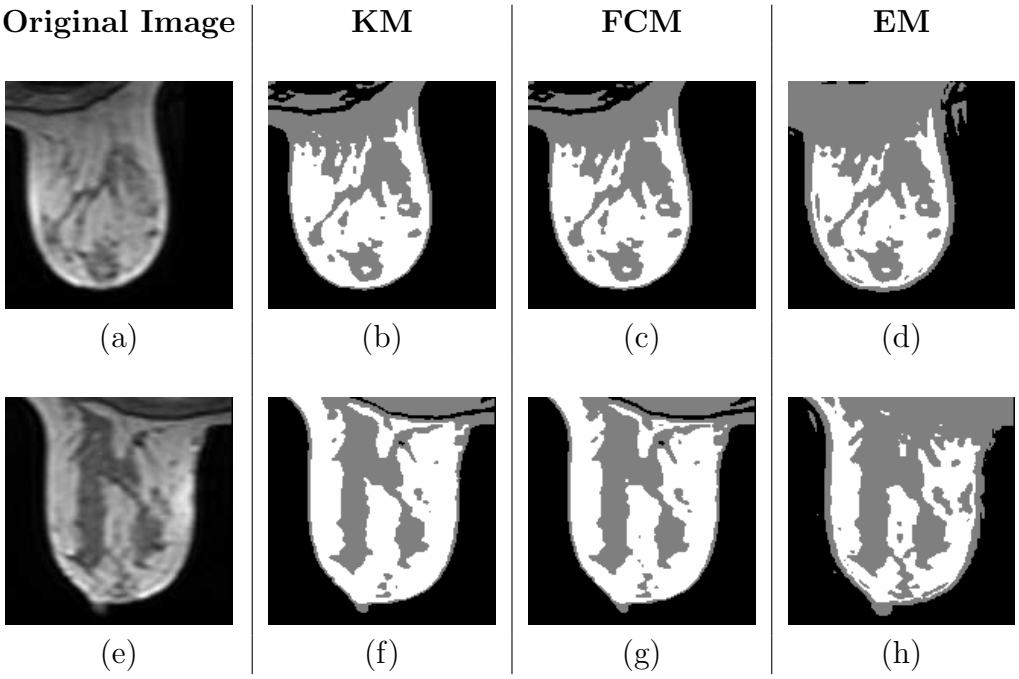

Figure 5.7: MRI segmentation results: (a,e) depicts original image, (b,f) K-Means algorithm, (c,g) Fuzzy-C Means and (d,h) EM algorithm.

A gold standard (manual segmentation done by an expert) is needed to accurately evaluate the segmentation result provide by each algorithm. Although this evaluation is not provided here, is our aim to perform experiments in that direction. The reason that this is not shown here is due to the difficulty of obtaining this kind of ground truth data in MR breast images. However by visual inspection, qualitative evaluation can be provided leading to the conclusion that K-means and Fuzzy C-means approaches obtain the better results. However and as stated earlier, further evaluation is desirable an will be provided as a future work.

5.4 Surface Breast Model

Previous sections 5.2 and 5.3 have shown a way to obtain breast profile and tissue classification from both modalities, MR and X-ray imaging. This information is used to obtain an initial geometrical representation of the breast. The geometrical modelling is the generation of surface models and is known as triangulation. Triangulated surfaces represent the boundaries between the different tissue regions. Surface models substantially reduce the original data amount and enable a compact representation of complex geometrical structures. After MR image segmentation, a process to extract the breast profile of the MR data is performed with the help of the Marching Cubes [85] algorithm. This algorithm uses the information at the corners of a voxel to construct a surface that approximates the original surface. The Marching Cubes algorithm is based on a set of patterns of surface-edge intersections (see Figure 5.8) proposed by Lorensen [85] .

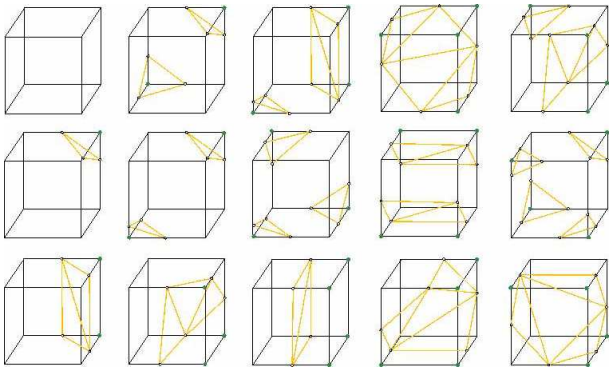

Figure 5.8: Marching Cubes algorithm: The 15 figures proposed in [85] to approximate the contour inside a voxel.

The basic principle of the Marching Cubes is to divide the 3D image into cubic cells (voxels) whose vertex are adjacent points of the image and to determine the intersection between the surface of the object and the cell. Considering that each vertex can be either inside or outside the object, there can be 256 different configurations that can be reduced to 15 when removing the ones that are identical except for a rotation or a symmetry. This gives us a surface described as a triangle mesh. The vertex normals are estimated as the average of the normal vectors of all the triangles that share the vertex.

In our case, MR slices have been segmented using the previously described K-

Means algorithm (Section 4.3.2) into three classes. Its union conforms the segmented breast volume represented by voxels. Contour transitions are easily distinguished, hence the Marching Cubes algorithm easily extracts the surfaces. Figure 5.9 shows the results of breast surface and the internal structures extraction results.

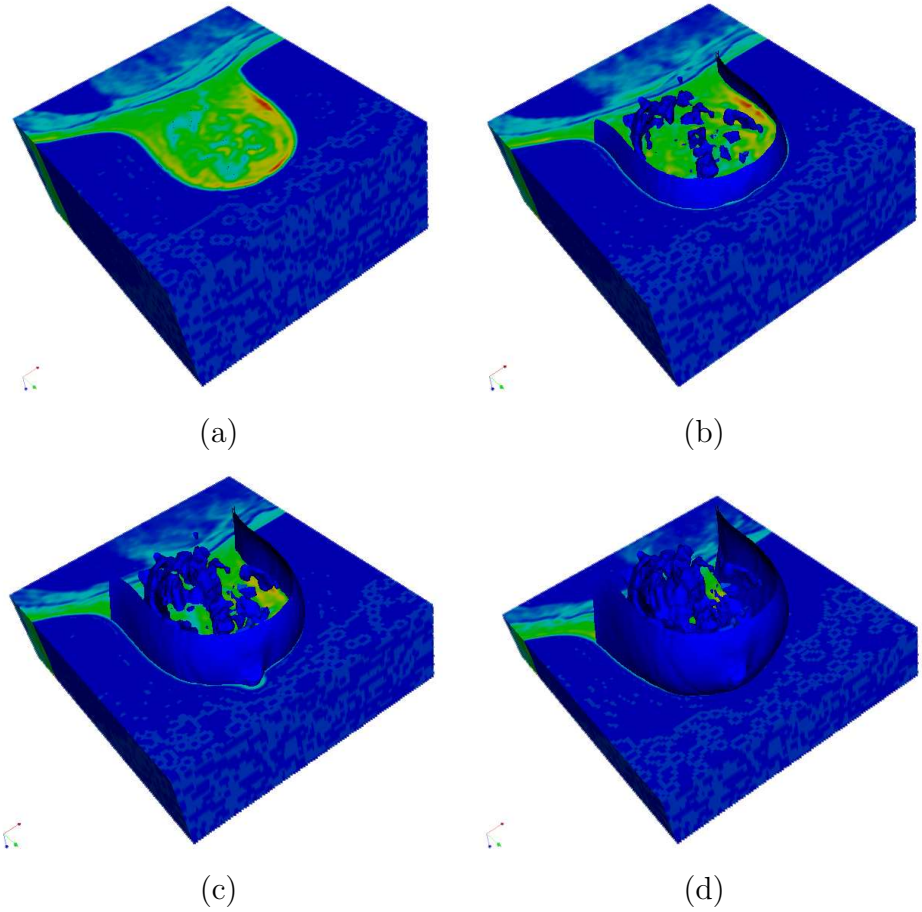

Figure 5.9: Cut view of the breast surface model. (a) Coloured breast MR data, (b-d) extracted contours from segmented MR slices.

Once surface is obtained from MR data, a preliminar breast model is obtained. Figure 5.10 shows some views of the 3-D rotated surface breast model. Note that not only breast contour but also internal regions are modeled and will be used to simulate breast behaviour under compression.

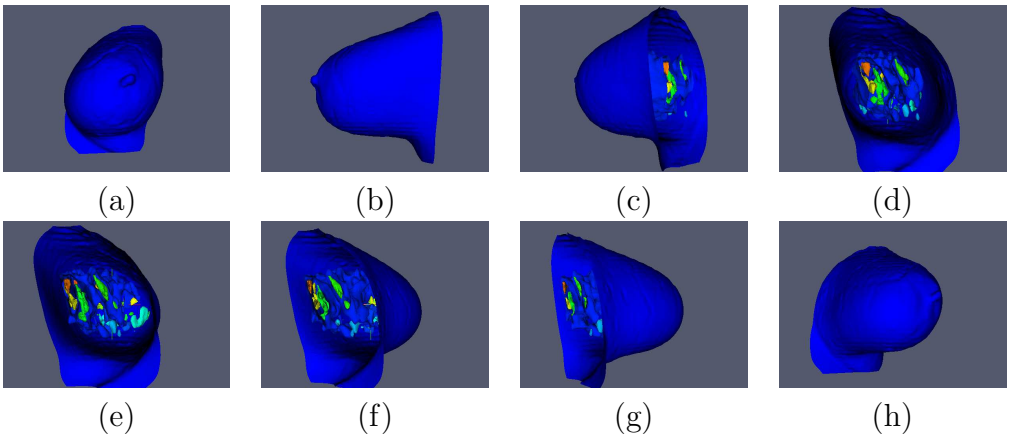

Figure 5.10: Sequence of images captured (a-h) from the 3-D rotated model. Images have been coloured to facilitate its visualisation. External blue surface depicts the breast boundary and internal coloured contouns depict the modeled parenchymal tissue.

5.5 Conclusions

This Chapter has presented undergoing work on building breast models for muti-modal correspondence. Various novel aspects have been provided in the initial steps prior to modelling: breast segmentation and tissue classification. Our method to classify breast tissue is based on the integration of texture and grey level information. An initial method based on gray-level information starts segmenting the profile of the breast. Subsequently, the Fuzzy C-Means algorithm is used to segment the different tissue types in the mammograms. Morphological and texture features are extracted to characterise the breast tissue for each cluster. Finally, kNN is used to classify the breast into MIAS annoted categories. Experimental results demonstrate the effectiveness of the proposed strategy. Further work will focus on the study of how to improve this classifier in order to take advantage of the fact that it has different performances on the distinct cases of breast density.

Tissue classification was additionally applied to MR volumes. Three clustering algorithms has been tested in order to classify the tissue. An evaluation of accuracy has kept in mind for further investigation. The MR acquisition process allows to obtain the non-compressed breast geometry. This is the basis of our geometry modelling system for breast profile and internal structures.

Based on fetures extracted from the MR image, a preliminar breast surface model

(3-D mesh) has been obtained. This model incorporates breast surface geometry and parenchymal tissue distribution. Fatty tissue is not modeled due to the fact that its position is assumed between breast skin and parenchymal tissue.

The future work of this thesis will be focused on using the extracted information into a realistic deformable model and provide a framework for multi-modal correspondence of MR and X-ray images. This future work if further analysed in the next Chapter.

Chapter 6

Thesis Planning

Once the initial steps of building a breast model have been achieved, research will be directed towards the integration of a deformable model to be able to simulate large deformations and thereupon to correspond multi-modal images. In this Chapter, the thesis line and the thesis planning are both presented. Moreover, scheduling with the developed work and the remainder work is shown.

6.1 Objectives

The main aim is to obtain a realistic breast model and to obtain correspondence between various imaging modalities including X-ray, MRI and US. The correspondence should be based on matching meaningful internal structures in addition to using image correlation (similarity criteria).

This model will provide a useful tool for the detection and evaluation of the breast cancer development. Another possible application is found in the registration of mammograms, MR images and ultrasound images. These three imaging types are used in diagnosis and biopsy of the lesions in the breast tissue. An accurate model of the breast would be able to combine the information of these images automatically. Moreover, the model could be used as a radiologist guiding device in real-time surgical procedures such as biopsy. Finally, thanks to the ability of the application to gather all the available information in a common model, it will also be possible to use it as a learning tool for the novice radiologist when exploring known prototype cases. All those possible applications are depicted in Figure 6.1.

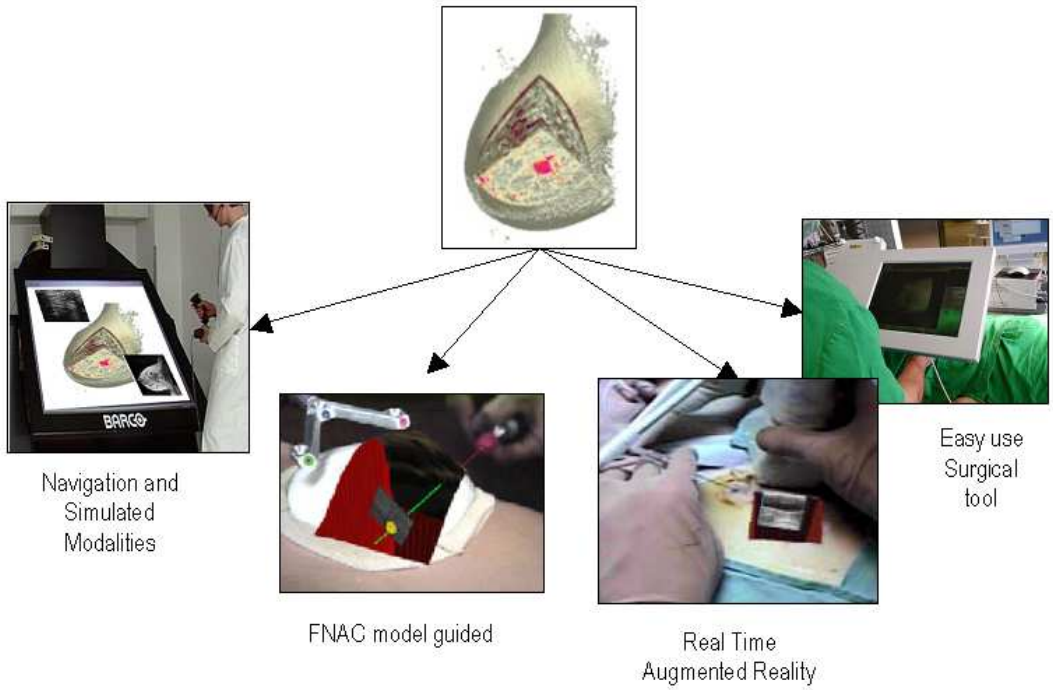

Figure 6.1: Applications of the breast model.

The steps will done towards its realisation are discussed as follows.

Feature Extraction An automated method to segment the digital mammogram into breast region and background with a new pectoral muscle suppression technique and a tissue classification approach have been presented using X-ray Mammograms. Tissue types in MR imaging have been classified into fatty and glandular tissue.

It is our aim to investigate characterisation of ultrasound imaging. The use of position sensors attached to the ultrasound sensor will provide an absolute reference with which correlate our model and the ultrasonic image. The possibility of correlate both information with a sensor-less approach will be also studied.

Breast Modelling An strategy to automatic geometry extraction of breast has been proposed. Further efforts will be directed to apply a deformable modelling technique to this geometry.

A biomechanical model of female breast tissue, capable to simulate large de-

formations will be obtained. A realistic deformation will be applied to the model in order to match X-ray images using profile and internal structures.

The obtained breast model should be accurate and robust but also needs to be computationally efficient and applicable in real-time in order to be clinically available. Nevertheless this efficiency has to be carefully evaluated to minimise its impact on the accuracy of the model.

Testing the Model: Synthetic and Real experiments The accuracy of the model will be assessed in both synthetic and real experiments. A project called Truth Cube, which consists on providing a method and preliminary data for quantifying the accuracy of soft tissue models is being developed [73]. Our aim is to test our model using this framework a synthetic breast phantom, thus knowing the exact segmentation and deformations due to various compressions. A second test will investigate using real cases. A radiologist will perform various acquisitions with different compressions of the same breast. The deformable breast model will be tested simulating these compressions. Hence, its accuracy to handle with large deformations will be measured.

MRI *vs* Model correspondence The registration of real MR data of the breast with its model will be treated to study the possibility of build a breast atlas. An Atlas of breast imaging will provide a new tool to store the knowledge about breast cancer disease and provide radiologist with novel training and diagnosis tools.

X-ray *vs* Model correspondence The correspondence of a lesion in MLO and CC view mammograms done in already published works (ie. Yam *et al.* [151]), is thought to be improved by the inclusion of a breast model. We will evaluate the increase of the accuracy of the lesion correspondence between views.

The registration of X-ray mammograms with MR imaging as done by Behenbruch, Martí and Ruiter used projection techniques to simulate an X-ray. We will try to improve the projective model incorporating a perspective projection and assigning different attenuation coefficient depending of the type of tissue in the MR image based on a more accurate tissue classification. We will take into account the energy needed to generate an X-ray mammogram as well as the compression factor, information that is available from the standard DICOM header of Full Field Digital Mammographic Systems. We will try to

find correspondence between internal structures present inside the MR and the X-ray mammogram.

US *vs* Model Correspondence The simulation of ultrasound imaging using the breast model will be studied. It would help the sensor-less correlation between the breast model and ultrasound data.

Chapter 7

Related Publications

The work developed in the last two years within the Computer Vision and Robotics Group at the University of Girona has led to several publications in the field of Computer Vision. Practically all of them have specifically focused on Mammography Imaging.

Articles in Conferences

- D. Raba, A. Oliver, R. Martí, M. Peracaula, J. Espunya. Breast Segmentation with Pectoral Muscle Suppression on Digital Mammograms. In *Iberian Conference on Pattern Recognition and Image Analysis* [**IbPRIA 2005**] vol.35-23 pp.471-478. Estoril, Portugal. June 2005.

- D. Raba, J. Martí, R. Martí, M. Peracaula. Breast mammography asymmetry estimation based on fractal and texture analysis. In *Computed Aided Radiology and Surgery* [**CARS 2005**]. Vol. 1281C, pp.1397. Berlin, Germany. June 2005.

- A. Oliver, J. Freixenet, A. Bosch, D. Raba, R. Zwiggelaar. Automatic Classification of Breast Tissue. In *Iberian Conference on Pattern Recognition and Image Analysis* [**IbPRIA 2005**] vol.35-23 pp.431-438. Estoril, Portugal. June 2005.

- J. Freixenet, D. Raba, A. Oliver, J. Espunya. Breast profile segmentation based on the region growing approach. In *Computed Aided Radiology and*

Surgery [**CARS 2005**]. Vol. 1281C, pp.1385. Berlin, Germany, June 2005.

- J. Martí, J. Freixenet, M. Peracaula, A. Oliver, D. Raba, J. Espunya, J. Pont, R. Martí. Automatic segmentation of microcalcifications based on the fusion of different algorithms over CC and MLO views. In *International Workshop on Digital Mammography* [**IWDM 2004**]. Chapel Hill, North Carolina. June 2004

- J. Pont, J. Martí, R. Bassaganyas, D. Raba, R. Martí, A. Oliver, M. Peracaula, J. Espunya, E. Golabardes, J. Freixenet. Cerca de documentació complementària en bases de dades de mamografies digitals per ajudar en el diagnòstic precoç. In *Congrés Català de Sinologia i Patologia Mamària* [**CCSPM 2004**]. Girona, Catalonia, May 2004.

- R. Zwiggelaar, L. Blot, D. Raba, ERE. Denton. Set-Permutation-Occurrence Matrix based Texture Segmentation. In *Iberian Conference On Pattern Recognition and Image Analysis* [**IbPRIA 2003**], pp. 1099-1107. Mallorca, Spain. June 2003

- R. Zwiggelaar, L. Blot, D. Raba, ERE. Denton. Texture Segmentation in Mammograms. In *Medical Image Understanding and Analysis* [**MIUA 2003**] pp.137-140. Sheffield, UK. June 2003.

- J. Martí, J. Freixenet, D. Raba, A. Bosch, J. Pont. HRIMAC una Herramienta de Recuperación de Imágenes Mamográficas por Análisis del Contenido para el Asesoramiento del Cáncer de Mama, In *Informática de la salud* [**IS 2003**], pp.56-61, Madrid, Spain. June 2003.

- J. Freixenet, X. Muñoz, D. Raba, J. Martí, X. Cufí. Yet Another Survey on Image Segmentation: Region and Boundary Information Integration. In *European Conference on Computer Vision* [**ECCV 2002**]. vol.III, p.408-422, Copenhagen, Denmark. May, 2002.

- X. Muñoz, J. Freixenet, D. Raba, X. Cufí, J. Martí. Region-Boundary Cooperative Image Segmentation Based on Active Regions. In *Congres Català d'Intel.ligència Artificial* [**CCIA 2002**]. Castelló de la Plana, Spain. October 2002.

Bibliography

[1] M. Abdel-Mottaleb and C. Carman. Locating the boundary between the breast skin edge and the background in digitized mammograms. In *Proc International Workshop on Digital Mammography*, pages 467–470, 1996.

[2] M. Amrani, F. Jaillet, M. Melkemi, and B. Shariat. Simulation of deformable organs with a hybrid approach. *Revue Int. d'infographie et de la CFAO*, 16(2), September 2001.

[3] M. Amrani and B. Shariat. Deformable organs modeling with multi layer particle systems. In *Proc IEEE International Conference on Information Visualization*, volume 7695, pages 351–356, July 2000.

[4] M. Anderson, R. Boulic, and D. Thalmann. Deformable tissue parameterized by properties of real biological tissue. In *Proc International Symposium on Surgery Simulation and Soft Tissue Modeling*, pages 74–87, 2003.

[5] F. Azar, D. Metaxas, and M. Schnall. A finite element model of the breast for predicting mechanical deformations during biopsy procedures. In *Proc IEEE Workshop on Mathematical Methods in Biomedical Image Analysis*, pages 38–45, 2000.

[6] P. Bakic. *Breast Tissue Description and Modeling in Mammography.* Phd thesis, Lehigh University, PA, USA, 2000.

[7] R. Balaniuk and J. Salisbury. Soft-tissue simulation using the radial elements method. In *Proc International Symposium on Surgery Simulation and Soft Tissue Modeling*, pages 48–58, Juan-Les-Pins, France, 2003.

[8] A. Barr. Global and local deformations of solid primitives. In *Proc International Conference on Computer Graphics and Interactive Techniques*, pages 21–30, 1984.

[9] R. Bartels, J. Beatty, and B. Barsky. *An Introduction to Splines for use in Computer Graphics and Geometric Models*. Morgan Kaufmann, 1987.

[10] V. Baudet, F. Jaillet, and B. Shariat. Fitting a 3D particle system model to a non dense dataset. In *Proc International Conference on Geometry and Graphics*, volume 1, pages 210–220, July 2002.

[11] C. Behrenbruch, K. Marias, P. Armitage, M. Yam, N. Moore, R. English, J. Clarke, and M. Brady. Fusion of contrast-enhanced breast MR and mammographic imaging data. *Medical Image Analysis*, 7(3):"311–340", September 2003.

[12] J. Bezdek. *Pattern Recognition With Fuzzy Objective Function Algorithms*. Plenum Press, New York, 1981.

[13] U. Bick and M. Giger. Automated segmentation of digitized mammograms. *Academic Radiology*, 2:1–9, 1995.

[14] L. Blot and R. Zwiggelaar. Background texture extraction for the classification of mammographic parenchymal patterns. In *Proc Medical Image Understanding and Analysis*, pages 145–148, 2001.

[15] F. Bookstein. Principal warps: Thin-plate splines and the decomposition of deformations. *IEEE Transactions on Pattern Analysis and Machine Intelligence*, 11:567–585, 1989.

[16] K. Bovis and S. Singh. Classification of mammographic breast density using a combined classifier paradigm. In *Proc International Workshop on Digital Mammography*, pages 177–180, 2002.

[17] N. Boyd, J. Byng, R. Jong, E. Fishell, L. Little, A. Miller, G. Lockwood, D. Tritchler, and M. Yaffe. Quantitative classification of mammographic densi-

ties and breast cancer risk: results from the canadian national breast screening study. *Journal of the National Cancer Institute*, 87:670–675, 1995.

[18] D. Breen. *A Particle-Based Model for Simulating the Draping Behavior of Woven Cloth.* doctoral dissertation, Rensselaer Polytechnic Inst., 1993.

[19] M. Bro-Nielsen and S. Cotin. Real-time volumetric deformable models for surgery simulation using finite elements and condensation. *Computer Graphics Forum*, 15(3):57–66, 1996.

[20] D. Buckley, R. Kerslake, J. Blackband, and A. Horsman. Quantitative analysis of multislice gd-dtpa enhancement dynamic MR images using an automated simplex minimisation procedure. *Magnetic Resonance in Medicine*, 32:646–651, 1994.

[21] J. Byng, N. Boyd, E. Fishell, R. Jong, and M. Yaffe. Automated analysis of mammographic densities. *Physics in Medicine and Biology*, 41:909–923, 1996.

[22] C. Caldwell, S. Stapleton, D. Holdsworth, R. Jong, W. Weiser, G. Cooke, and M. Yaffe. Characterization of mammographic parenchymal pattern by fractal dimension. *Physics in Medicine and Biology*, 35:235–247, 1990.

[23] R. Chandrasekhar and Y. Attikiouzel. Gross segmentation of mammograms using a polynomial model. In *Proc IEEE Engineering in Medicine and Biology Society*, volume 3, pages 1056–1058, 1996.

[24] D. Chen and D. Zeltzer. Pump it up: Computer animation of a biomechanically based model of muscle using the finite element method. In *Proc International Conference on Computer Graphics and Interactive Techniques*, pages 89–98, 1992.

[25] J. Christensen, J. Marks, and J. Ngo. Automatic motion synthesis for 3D mass-spring models. Technical Report 1, MERL: The Visual Computer, January 1997.

[26] J. Clin. American cancer society guidelines for breast cancer screening: Update 2003. *Cancer*, 53:141–169, 2003.

[27] T. Cootes and C. Taylor. Active shape models - smart snakes. In *Proc British Machine Vision Conference*, pages 266–275, UK, September 1992.

[28] S. Coquillart. Extended free-form deformation: a sculpturing tool for 3D geometric modeling. In *Proc International Conference on Computer Graphics and Interactive Techniques*, pages 187–196, 1990.

[29] I. Costa and R. Balaniuk. LEM - an approach for real time physically based soft tissue simulation. In *Proc IEEE International Conference on Robotics and Automation*, pages 2337–2343, Seoul, Korea, May 2001.

[30] S. Cotin and H. Delingette. Real-time surgery simulation with haptic feedback using finite elements. *Proc IEEE International Conference on Robotics and Automation*, pages 3739–3744, 1998.

[31] S. Cotin, H. Delingette, and N. Ayache. Real-time elastic deformations of soft tissues for surgery simulation. *IEEE Transactions on Visualization and Computer Graphics*, 5(1):62–73, 1999.

[32] I. Céspedes, J. Ophir, H. Ponnekanti, and N. Maklad. Elastography: Elasticity imaging using ultrasound with application to muscle and breast in vivo. *Ultrasonic Imaging*, 15:73–88, 1993.

[33] G. Debunne. *Animation multirésolution d'objets déformables en temps-réel, Application à la simulation chirurgicale.* PhD thesis, Institut National Polytechnique de Grenoble, France, December 2000.

[34] G. Debunne, M. Desbrun, M. Cani, and A. Barr. Dynamic real-time deformations using space and time adaptive sampling. In *Computer Graphics Proceedings*, Annual Conference Series. ACM Press, August 2001.

[35] H. Delingette. Towards realistic soft-tissue modeling in medical simulation. In *Proceedings of the IEEE*, volume 86, pages 512–523, 1998.

[36] H. Delingette, S. Cotin, and N. Ayache. A hybrid elastic model allowing real-time cutting, deformations and force-feedback for surgery training and simulation. *Computer Animation*, 23(6):26–28, May 1999.

[37] A. Dempster, N. Laird, and D. Rubin. Maximum-likelihood from incomplete data via EM algorithm. *Journal of the Royal Statistical Society: Series B*, pages 1–38, 1977.

[38] M. Desco, J. López, C. Benito, A. Santos, P. Domínguez, S. Reig, C. Arango, and C. García-Barreno. A multimodality workstation in practice. *Proc International Symposium and Exhibition of Computer Assisted Radiology and Surgery*, pages 218–222, 1999.

[39] C. D'Orsy. Early detection of breast cancer: mammography. *Breast Cancer Research*, 18(1):107–109, 1991.

[40] R. Duda, P. Hart, and D. Stork. *Pattern Classification*. John Wiley & Sons, New York, 2 edition, 2001.

[41] P. Ell and G. Schulthess. PET/CT: a new road map. *European Journal of Nuclear Medicine and Molecular Imaging*, 29(6):719–720, June 2002.

[42] R. Ferrari and R. Rangayyan. Automatic identification of the pectoral muscle in mammograms. *IEEE Transactions on Medical Imaging*, 23(2):232–245, 2000.

[43] R. Ferrari and R. Rangayyan. Segmentation of mammograms: Identification of the skin boundary and the pectoral muscle. In *Proc International Workshop on Digital Mammography*, volume 23, 2000.

[44] J. Freixenet, X. Muñoz, D. Raba, J. Martí, and X. Cufí. Yet another survey on image segmentation: Region and boundary information integration. In *Proc European Conference on Computer Vision*, volume III, pages 408–422, Copenhagen, Denmark, May 2002.

[45] Y. Fung. *Biomechanics: Mechanical Properties of Living Tissues*. 2nd ed. Berlin: Springer-Verlag, 1993.

[46] A. Galea and R. Howe. Mammography registered tactile imaging. In *Proc International Symposium on Surgery Simulation and Soft Tissue Modeling*, pages 183–193, 2003.

[47] P. Gamagami. *Atlas of Mammography: New Early Signs in Breast Cancer*. Blackwell Science, 1996.

[48] F. Georgsson. *Algorithms and Techniques for Computer Aided Mammographic Screening*. PhD thesis, UMINF-01.15, Umeå University, Sweden, 2001.

[49] S. Gibson, J. Samosky, and A. Mor. Simulating arthroscopic knee surgery using volumetric object representations, real-time volume rendering and haptic feedback. In *Proc of CVRMed-MRCAS*, pages 369–378, London, UK, 1997. Springer-Verlag.

[50] M. Goodsitt and H. Chan. Classification of compressed breast shapes for the design of equalisation filters in X-ray mammography. *Medical Physics*, 25(6):937–947, 1998.

[51] E. Grinspun, P. Krysl, and P. Schroder. Charms: a simple framework for adaptive simulation. In *Proc International Conference on Computer Graphics and Interactive Techniques*, pages 281–290, 2002.

[52] S. Hajnal, P. Taylor, M. Dilhuydy, B. Barreau, and J. Fox. Classification of mammograms by density: rationale and preliminary results. In *Proc. SPIE*, volume 1905, pages 478–489, 1993.

[53] R. Haralick, K. Shanmugan, and I. Dunstein. Textural features for image classification. *IEEE Transactions on Systems, Man, and Cybernetics*, 3(6):610–621, 1973.

[54] M. Hauth. *Visual simulation of deformable models*. PhD thesis, Universität Tübingen, Germany, 2004.

[55] J. Hein and M. Kallergi. Multiresolution wavelet approach for separating the breast region from the background in high resolution digital mammography. In *Proc International Workshop on Digital Mammography*, pages 295–298, Nijmegen, 1998.

[56] S. Heywang-Köbrunner, D. Dershaw, and I. Schreer. *Diagnostic Breast Imaging. Mammography, Sonography, Magnetic Resonance Imaging, and Interventional Procedures*. Thieme, Stuttgart, Germany, 2001.

[57] R. Highman, J. Brady, and B. Shepstone. A representation for mammographic image processing. *Medical Image Analysis*, 1(1):1–18, 1996.

[58] R. Highnam, Y. Kita, M. Brady, B. Shepstone, and R. English. Determining correspondence between views. In *Proc International Workshop on Digital Mammography*, pages 111–118, June 1998.

[59] W. Ho and P. Lam. Clinical performance of computer-assisted detection (CAD) system in detecting carcinoma in breasts of different densities. *Clinical Radiology*, 58:133–136, 2003.

[60] A. Hoyer and W. Spiesberg. Computerized mammogram processing. In *Phillips Technical Review*, volume 38, pages 347–355, 1979.

[61] W. Hsu, J. Hughes, and H. Kaufman. Direct manipulation of free-form deformations. In *Proc International Conference on Computer Graphics and Interactive Techniques*, pages 177–184, 1992.

[62] K. Hui and H. Leung. Virtual sculpting and deformable volume modelling. In *Proc IEEE International Conference on Information Visualization*, pages 664–669, London, England, UK, 2002.

[63] N. Ibrahim and H. Fujita. Automated detection of clustered microcalcifications on mammograms: CAD system application to MIAS database. *Physics in Medicine and Biology*, 42(12):2577–2589, 1997.

[64] Imaginis. Imaginis: The breast health resource. http://imaginis.com/, 2004.

[65] F. Jaillet, B. Shariat, and D. Vandorpe. Deformable object reconstruction with particle systems. *Computers and Graphics*, 22(2-3):189–194, March 2003.

[66] A. Jain, M. Murty, and P. Flynn. Data clustering: A review. *ACM: Computing Surveys*, 31(3):264–323, 1999.

[67] D. James and D. Pai. Artdefo: accurate real time deformable objects. In *Proceedings of conference on Computer graphics and interactive techniques*, pages 65–72, New York, USA, 1999. ACM Press/Addison-Wesley Publishing Co.

[68] P. Jannin, O. Fleig, E. Seigneuret, C. Grova, X. Morandi, and J. Scarabin. A data fusion environment for multimodal and multi-informational neuronavigation. *Journal of Computer Aided Surgery*, 5(1):1–10, 2000.

[69] J. Jenne, R. Rastert, I. Simiantonakis, J. Debus, and P. Huber. MRI guided focused ultrasound surgery for the treatment of breast cancer. In *Proc IEEE Ultrasonics Symposium*, volume 2, pages 1377–1380, Atlanta, GA, USA, 2001.

[70] R. Jong, M. Yaffe, M. Skarpathiotakis, R. Shumak, N. Danjoux, A. Gunesekara, and D. Plewes. Contrast-enhanced digital mammography: Initial clinical experienc. *Radiology*, 228(3):842–850, July 2003.

[71] N. Karssemeijer and G. te Brake. Combining single view features and asymmetry for detection of mass lesions. In *Proc International Workshop on Digital Mammography*, pages 95–102, June 1998.

[72] E. Keeve, S. Girod, and B. Girod. Craniofacial surgical simulation. In *International Conference on Visualization in Biomedical Computing*, pages 541–546, 1996.

[73] A. Kerdok, S. Cotin, M. Ottensmeyer, A. Galea, R. Howe, and S. Dawson. Truth cube: Establishing physical standards for real time soft tissue simulation. *Medical Image Analysis*, 7:283–291, 2003.

[74] Y. Kita. Elastic-model driven analysis of several views of a deformable cylindrical object. *IEEE Transactions on Pattern Analysis and Machine Intelligence*, 18(12):1150–1162, December 1996.

[75] M. Kossoff. Ultrasound of the breast. *World Journal of Surgery*, 24(2):143–157, February 2000.

[76] A. Krishnan, M. Schell, Y. Yu, and W. O'Dell. 3D FEM to predict deformation during brachytherapy needle insertion. In *AAPM Meeting*, July 2004.

[77] T. Krouskop, R. Price, T. Wheeler, and P. Younes. Modulus variations in breast tissues. In *Proc International Conference of the Ultrasonics Measurements and Imaging of Tissue Elasticity*, Niagara Falls, 2002.

[78] S. Kwok, R. Chandrasekhar, and Y. Attikiouzel. Automatic pectoral muscle segmentation on mammograms by straight line estimation and cliff detection. In *Proc International Conference on Information and Intelligent Systems*, pages 67–72, November 2001.

[79] J. Lamarque. *Digitalización en mamografía*. Edit. Díaz de Santos, 1995.

[80] T. Lau and W. Bischof. Automated detection of breast tumors using the asymmetriy approach. *Computers and Biomedical Research*, 24(3):273–295, 1991.

[81] J. Lewin, P. Isaacs, V. Vance, and F. Larke. A new method for 3D reconstruction in digital tomosynthesis. *Radiology*, July 2003.

[82] Y. Li and K. Brodlie. Soft object modelling with generalised chainmail - extending the boundaries of web-based graphics. *Computer Graphics Forum*, 22(4):717–728, 2003.

[83] H. Liu, L. Sun, G. Wang, and M. Vannier. Analytic modeling of breast elastography. *Medical Physics*, 30(9):2340–2349, September 2003.

[84] S. Lloyd. Least squares quantization in PCM. *IEEE Transactions on Information Theory*, 28(2):129–136, 1982.

[85] W. Lorensen and H. Cline. Marching cubes: A high resolution 3D surface construction algorithm. In *Proc International Conference on Computer Graphics and Interactive Techniques*, pages 163–169, 1987.

[86] J. MacQueen. Some methods of classification and analysis of multivariate observations. In *Proceedings of the Fifth Berkeley Symposium on Mathematical Statistics and Probability*, volume 1, pages 281–297, 1967.

[87] J. Maintz and M. Viergever. A survey of medical image registration. *Medical Image Analysis*, 2:1–36, March 1998.

[88] S. Malur, S. Wurdinger, A. Moritz, W. Michels, and A. Schneider. Comparison of written reports of mammography, sonography and magnetic resonance mammography for preoperative evaluation of breast lesions, with special emphasis on magnetic resonance mammography. *Breast Cancer Research*, 3(1):55–60, 2001.

[89] K. Marias. *Registration and Quantitative Comparison of Temporal Mammograms (with Application to HRT data)*. PhD thesis, University College London, UK, 2002.

[90] R. Martí. *Image Registration Applied to Multi-Modality Mammography*. PhD thesis, University of East Anglia, UK, 2002.

[91] R. Martí, R. Zwiggelaar, and C. Rubin. Tracking mammographic structures over time. In *Proc British Machine Vision Conference*, pages 143–152, September 2001.

[92] M. Masek, Y. Attikiouzel, and C. de Silva. Skin-air interface extraction from mammograms using an automatic local thresholding algorithm. In *International Conference Biosignal*, pages 204–206, Brno, CR, June 2000.

[93] K. McLoughlin and P. Bones. Segmentation of the breast-air boundary for a digital mammogram image. In *Proc Image Vision Computing New Zealand*, 1996.

[94] A. Méndez and P. Tahoces. Automatic detection of breast border and nipple in digital mammograms. *Computer Methods and Programs in Biomedicine*, 49(3):253–262, 1996.

[95] P. Miller and S. Astley. Classification of breast tissue by texture and analysis. *Image and Vision Computing*, 10:227–282, 1992.

[96] A. Méndez and P. Tahoces. Computer-aided diagnósticos: detection of masses on digital mammograms. In *Proc International Workshop on Image and Signal Processing*, pages 465–468, Manchester, UK, 1996.

[97] A. Morton, H. Chan, and M. Goodsitt. Automated model-guided breast segmentation algorithm. *Medical Physics*, 23:1107–1108, 1996.

[98] L. Nedel and D. Thalmann. Real time muscle deformations using mass-spring systems. In *Proceedings of the Computer Graphics International*, pages 156–165, 1998.

[99] R. Nishikawa, M. Giger, K. Doi, C. Vyborny, and R. Schmidt. Computer-aided detection and diagnósticos of masses and clustered microcalcifications from digital mammograms. In *Proc International Workshop on Digital Mammography*, pages 82–102, 1994.

[100] A. C. of Radiology. *Illustrated Breast Imaging Reporting and Data System BIRADS*. American College of Radiology, 3rd edition, 1998.

[101] T. Ojala and J. Liang. Interactive segmentation of the breast region from digitized mammograms with united snakes. Technical Report 315, Turku Centre for Computer Science, Finland, 1999.

[102] S. Petroudi, T. Kadir, and M. Brady. Automatic classification of mammographic parenchymal patterns: A statistical approach. In *Proc IEEE Engineering in Medicine and Biology Society*, volume 2, pages 416–423, 2003.

[103] C. Piron, P. Causer, R. Jong, R. Shumak, and D. Plewes. A hybrid breast biopsy system combining ultrasound and MRI. *IEEE Transactions on Medical Imaging*, 22(9):1100–1110, 2003.

[104] J. Platt and A. Barr. Constraints methods for flexible models. In *Proc International Conference on Computer Graphics and Interactive Techniques*, pages 279–288. ACM Press, 1988.

[105] J. Pluim, J. Maintz, and M. Viergever. Mutual-information-based registration of medical images: a survey. *IEEE Transactions on Medical Imaging*, 22(8):986–1004, 2003.

[106] X. Provot. Deformation constraints in a mass-spring model to describe rigid cloth behavior. In W. Davis and P. Prusinkiewicz, editors, *Proc Graphics Interface*, pages 147–154, 1995.

[107] M. Puddephat. Principles of magnetic resonance imaging. http://www.easymeasure.co.uk/, 2002.

[108] Y. Qiu, D. Goldgof, L. Li, S. Sarkar, Y. Zhang, and S. Anton. Correspondence recovery in 2-view mammography. In *IEEE International Symposium on Biomedical Imaging: From Nano to Macro*, pages 197–200, Arlington, VA, USA, 2004.

[109] W. Reeves. Particle systems: A technique for modeling a class of fuzzy objects. *ACM Transactions on Graphics*, 2(2):91–108, 1983.

[110] H. Rickard, G. Tourassi, and A. Elmaghraby. Self-organizing maps for masking mammography images. In *Proc IEEE Engineering in Medicine and Biology Society*, pages 302–305, April 2003.

[111] L. Roose, W. De Maerteleire, W. Mollemans, and P. Suetens. Validation of different soft tissue simulation methods for breast augmentation. In *Proc International Symposium and Exhibition of Computer Assisted Radiology and Surgery*, pages 38–45, June 2005.

[112] D. Rueckert, L. Sonoda, C. Hayes, D. Hill, M. Leach, and D. Hawkes. Non-rigid registration using free-form deformations: Application to breast MR images. *IEEE Transactions on Medical Imaging*, 18(8):712–721, 1999.

[113] N. Ruiter. *Registration of X-ray Mammograms and MR-Volumes of the Female Breast based on Simulated Mammographic Deformation.* Dissertation, Mensch und Buch Verlag, Berlin, 2004.

[114] N. Ruiter, T. Müller, R. Stotzka, H. Gemmeke, J. Reichenbach, and W. Kaiser. Automatic image matching for breast cancer diagnostics by a 3D deformation model of the mamma. *Biomedizinische Technik*, 47(1):644–647, March 2002.

[115] P. Saha and J. Udupa. Breast tissue density quantification via digitized mammograms. *IEEE Transactions on Medical Imaging*, 20(8):792–803, Aug. 2001.

[116] A. Samani, J. Bishop, M. Yaffee, and D. Plewes. Biomechanical 3D finite element modeling of the human breast using MRI data. *IEEE Transactions on Medical Imaging*, 20(4):271–279, 2001.

[117] A. Santos, J. Pascau, M. Desco, C. Benito, F. García-Salazar, R. Carrillo, and P. García-Barreno. Neurosurgery for functional disorders guided by multimodality imaging. In *Proc SPIE Medical Imaging*, volume 4319, pages 277–285, 2001.

[118] L. Sanz and D. Petkovic. Machine vision algorithms for automated inspection of thin-film disk heads. *IEEE Transactions on Pattern Analysis and Machine Intelligence*, 10(6):830–848, 1988.

[119] J. Schnabel, D. Rueckert, M. Quist, J. Blackall, A. Castellano-Smith, T. Hartkens, G. Penney, W. Hall, H. Liu, C. Truwit, F. Gerritsen, D. Hill, and D. Hawkes. A generic framework for non-rigid registration based on non-uniform multi-level free-form deformations. In *Proc International Conference on Medical Image Computing and Computed Assisted Intervention*, pages 573–581, 2001.

[120] J. Schnabel, C. Tanner, A. Castellano-Smith, A. Degenhard, M. Leach, D. Hose, D. Hill, and D. Hawkes. Validation of non-rigid image registration sing finite element methods: Application to breast MR images. *IEEE Transactions on Medical Imaging*, 22(2):238–247, 2003.

[121] J. Sciarretta, A. Samani, J. Bishop, and D. Plewes. MR validation of soft tissue mimicing phantom deformation as modeled by nonlinear finite element analysis. *Medical Physics*, 29(1):65–72, January 2002.

[122] T. Sederberg and S. Parry. Free-form deformation of solid geometric models. In *Proc International Conference on Computer Graphics and Interactive Techniques*, pages 151–160, 1986.

[123] J. Semmlow and A. Shadagopappan. A fully automated system for screening xeromammograms. *Computers and Biomedical Reseach*, 13:350–362, 1980.

[124] F. Shtern. Digital mammography and related technologies: a perspective from the National Cancer Institute. *Radiology*, 183(3):629–630, 1992.

[125] K. Singh and E. Fiume. Wires: a geometric deformation technique. In *Proc International Conference on Computer Graphics and Interactive Techniques*, pages 405–414, 1998.

[126] R. Sivaramakrishna, N. Obuchowski, W. Chilcote, and K. Powell. Automatic segmentation of mammographic density. *Acad. Radiol.*, 8(3):250–256, 2001.

[127] E. Stomatakis and A. Cairns. A novel approach to aligning mammograms. In *Proc International Workshop on Digital Mammography*, pages 255–364, 1994.

[128] J. Suckling, D. Dance, E. Moskovic, D. Lewis, and S. Blacker. Segmentation of mammograms using multiple linked self-organizing neural networks. *Medical Physics*, 22:145–152, 1995.

[129] J. Suckling, J. Parker, D. Dance, S. Astley, I. Hutt, C. Boggis, I. Ricketts, E. Stamatakis, N. Cerneaz, S. Kok, P. Taylor, D. Betal, and J. Savage. The mammographic images analysis society digital mammogram database. In *Exerpta Medica, ICS*, volume 1069, pages 375–378, 1994.

[130] S. Suzuki, N. Suzuki, A. Hattori, A. Uchiyama, and S. Kobayashi. Sphere-filled organ model for virtual surgery system. *IEEE Transactions on Medical Imaging*, 23(6):714–722, June 2004.

[131] G. Székely, C. Brechbühler, J. Dual, R. Enzler, and J. Hug. Virtual reality-based simulation of endoscopic surgery. *Presence: Teleoperators and Virtual Environments*, 9(3):310–333, June 2000.

[132] R. Szeliski and D. Tonnesen. Surface modeling with oriented particle systems. In *Proc International Conference on Computer Graphics and Interactive Techniques*, pages 185–194, 1992.

[133] L. Tabar and P. Dean. *Teaching Atlas of Mammography.* Thieme, 2nd edition, 1985.

[134] P. Tahoces, J. Correa, M. Soutu, L. Gomez, and J. Vidal. Computer-assisted diagnosis: the classification of mammographic breast patterns. *Physics in Medicine and Biology*, 40:103–117, 1995.

[135] C. Tanner, A. Degenhard, J. Schnabel, A. Smith, C. Hayes, L. Sonoda, M. Leach, D. Hose, D. Hill, and D. Hawkes. A method for the comparison of biomechanical breast models. *Proc IEEE Workshop on Mathematical Methods in Biomedical Image Analysis*, pages 11–18, December 2001.

[136] P. Taylor, R. Owebs, and D. Ingram. 3D fractal modeling of breast growth. In *Proc International Workshop on Digital Mammography*, pages 785–791, June 2000.

[137] D. Terzopoulos, J. Platt, A. Barr, and K. Fleischer. Elastically deformable models. In *Proc International Conference on Computer Graphics and Interactive Techniques*, pages 205–214. ACM Press, July 1987.

[138] D. Terzopoulos, J. Platt, A. Barr, D. Zeltzer, A. Witkin, and J. Blinn. Physically-based modeling: Past, present, and future. In *Proc International Conference on Computer Graphics and Interactive Techniques*, volume 23, pages 191–209, 1989.

[139] D. L. Tonnesen. *Dynamically coupled particle systems for geometric modeling, reconstruction, and animation.* PhD thesis, University of Toronto, Canada, 1998. Adviser-Demetri Terzopoulos.

[140] C. Tromans, J. Brady, and R. Warren. A high accuracy technique for breast air boundary segmentation and the resulting improvement from its use in breast density estimation. In *Proc International Workshop on Digital Mammography*, pages 17–18, June 2004.

[141] P. Viola and W. Wells. Alignment by maximization of mutual information. In *Proc International Conference on Computer Vision*, page 16, Washington, DC, USA, 1995. IEEE Computer Society.

[142] C. Wagner, M. Schill, and R. Männer. Collision detection and tissue modeling in a vr-simulator for eye surgery. In *Proc of the Workshop on Virtual Environments*, pages 27–36, 2002.

[143] E. Warner, D. Plewes, R. S. Shumak, and M. Yaffe. Comparison of breast magnetic resonance imaging, mammography and ultrasound for surveillance of women at high risk for hereditary breast cancer. *Journal of Clinical Oncology*, 19(15):3524–3531, 2001.

[144] P. Wellman. *Tactile Imaging*. Doctoral thesis, Division of Engineering and Applied Sciences, Harvard University, MA, USA, 1999.

[145] D. Winfields, M. Silbiger, G. Brown, L. Clarke, S. Dwyer, M. Yaffe, and F. Shtern. Digital mammography and related technologies: a perspective from the National Cancer Institute. *Report of the Joint National Cancer Institute*, 29(4):507–515, 1994.

[146] M. Wirth. *A Nonrigid Approach to Medical Image Registration: Matching Images of the Breast*. Ph.d. thesis, RMIT University, Melbourne, Australia, 2000.

[147] M. Wirth, J. Lyon, and D. Nikitenko. A fuzzy approach to segmenting the breast region in mammograms. In *Proc North American Fuzzy Information Processing Society*, volume 1, pages 474–479, June 2004.

[148] M. Wirth and A. Stapinski. Segmentation of the breast region in mammograms using snakes. In *Canadian Conference on Computer and Robot Vision*, pages 385–392, May 2004.

[149] J. Wolfe. Risk for breast cancer development determined by mammographic parenchymal pattern. *Cancer*, 37:2486–2492, 1976.

[150] X. Wu, M. Downes, T. Goktekin, and F. Tendick. Adaptive nonlinear finite elements for deformable body simulation using dynamic progressive meshes. *Computer Graphics Forum*, 20(3):349–358, 2001.

[151] M. Yam and M. Brady. Three-dimensional reconstruction of microcalcifications clusters from two mammographic views. In *Proc Medical Image*, volume 20, pages 479–489, 2001.

[152] F. Yin, M. Giger, K. Doi, C. Vyborny, and R. Schmidt. Computerized detection of masses in digital mammograms: Analysis of bilateral subtraction images. *Medical Physics*, 18(5):955–963, 1991.

[153] H. Yserentant. On the multilevel splitting of finite element spaces. *Numerische Mathematik*, 49:379–412, 1986.

[154] C. Zhou, H. Chan, N. Petrick, M. Helvie, M. Goodsitt, B. Sahiner, and L. Hadjiiski. Computerized image analysis: Estimation of breast density on mammograms. *Medical Physics*, 28(6):1056–1069, 2001.

[155] Y. Zhuang and J. Canny. Real-time simulation of physically realistic global deformation. In *Proc IEEE International Conference on Information Visualization*, San Francisco, California, October 1999.

[156] B. Zitová and J. Flusser. Image registration methods: a survey. *Image and Vision Computing*, 21:977–1000, October 2003.

[157] R. Zwiggelaar, L. Blot, D. Raba, and E. R. Denton. Set-permutation-occurrence matrix based texture segmentation. In *Iberian Conference On Pattern Recognition and Image Analysis*, Mallorca, Spain, June 2003.

[158] R. Zwiggelaar and E. Denton. Optimal segmentation of mammographic images. In *Proc International Workshop on Digital Mammography*, 2004.